EUROFUSION WPJET1-PR(14) 11984

C Guillemaut et al.

Influence of atomic physics on EDGE2D-EIRENE simulations of JET divertor detachment with carbon and beryllium/tungsten PFCs

Preprint of Paper to be submitted for publication in Nuclear Fusion

This work has been carried out within the framework of the EUROfusion Consortium and has received funding from the Euratom research and training programme 2014-2018 under grant agreement No 633053. The views and opinions expressed herein do not necessarily reflect those of the European Commission.

Influence of Atomic Physics on EDGE2D-EIRENE Simulations of JET Divertor Detachment with Carbon and Beryllium/Tungsten Plasma-Facing Components

C. Guillemaut[1], R.A. Pitts[2], A.S. Kukushkin[2], J.P. Gunn[1], J. Bucalossi[1], G. Arnoux[3], P. Belo[4], S. Brezinsek[5], M. Brix[3], G. Corrigan[3], S. Devaux[3], J. Flanagan[3], M. Groth[6], D. Harting[5], A. Huber[5], S. Jachmich[7], U. Kruezi[5], M. Lehnen[5], S. Marsen[8], A.G. Meigs[3], O. Meyer[1], M. Stamp[3], J.D. Strachan[9], S. Wiesen[5], M. Wischmeier[10] and JET EFDA contributors*

JET-EFDA, Culham Science Centre, OX14 3DB, Abingdon, UK

[1]CEA, IRFM, F-13108 Saint-Paul-lez-Durance, France
[2]ITER Organization, Route de Vinon sur Verdon, 13115 Saint-Paul-Lez-Durance, France
[3]EURATOM-CCFE Fusion Association, Culham Science Centre, OX14 3DB, Abingdon, OXON, UK
[4]Institute of Plasmas and Nuclear Fusion, Association EURATOM-IST, Lisbon, Portugal
[5]Institut fur Plasmaphysik, Forschungszentrum Juelich GmbH, EURATOM Association, Trilateral Euregio Cluster, D-52425 Juelich, Germany
[6]Aalto University, Association EURATOM-Tekes, Otakaari 4, 02015 Espoo, Finland
[7]Laboratory for Plasma Physics, ERM/KMS, Association EURATOM-Belgian State, B-1000 Brussels, Belgium
[8]Max-Planck-Institut für Plasmaphysik, Teilinsitut Greifswald, EURATOMAssoziation, D-17491 Greifswald, Germany
[9]PPPL, Princeton University, Princeton, NJ 08540, USA
[10]Max-Planck-Institut für Plasmaphysik, EURATOM-Association, Boltzmannstr. 2, D-85748 Garching, Germany
** See annex of F. Romanelli et al, "Overview of JET Results", (24th IAEA Fusion Energy Conference, San Diego, USA (2012)).*

Preprint of Paper to be submitted for publication in
Nuclear Fusion

ABSTRACT

The EDGE2D-EIRENE code is applied for simulation of divertor detachment during matched density ramp experiments in high triangularity, L-mode plasmas in both JETC and JET-ILW. The code runs without drifts and includes either C or Be as impurity, but not W, assuming that the W targets have been coated with Be via main chamber migration. The simulations reproduce reasonably well the observed particle flux detachment as density is raised in both JET-C and JET-ILW experiments and can better match the experimental in-out divertor target power asymmetry if the heat flux entering the outer divertor is artificially set at around 2-3 times that entering the inner divertor. A careful comparison between different sets of atomic physics processes used in EIRENE shows that ion-molecule elastic collisions are required for the detachment seen in the EDGE2D-EIRENE simulations. This process provides good neutral confinement in the divertor at low temperature inherent for detachment. Comparison between EDGE2D-EIRENE and SOLPS4.3 simulations of the density ramp in C shows that the detachment trends are similar, but the importance of the ionmolecule elastic collisions is reduced in SOLPS4.3. Both codes suggest that any process capable of improving the neutral confinement in the divertor should help to improve the modelling of the detachment. A further outcome of this work has been to demonstrate that key JET divertor diagnostic signals – Langmuir probe electron temperatures and bolometric tomographic reconstructions – are running in the limit of validity in high recycling and detached conditions and cannot be reliably used for code validation. The simulations do, however, reproduce rather well the evolution of the line integrated bolometer chord measurements. Estimates made with a model accounting for plasma resistivity can also bring the electron temperature derived from Langmuir probes closer to the simulation results. The comparison between the code results and high-n Balmer line radiation intensity profiles indicates that a strong volume recombination source is present during the detachment and may play a role in this process.

1. INTRODUCTION

Partially detached divertor operation will be mandatory on ITER during burning plasma operations at Q = 10 to maintain the target power loading at technologically manageable levels [1]. Such regimes are found on essentially all divertor tokamaks, but are still not straightforward to reproduce in modelling (see, for example [2-4]).

In the study reported here, the EDGE2D-EIRENE code (2D fluid plasma + 3D kinetic Monte-Carlo neutrals) [5,6] is used to simulate detachment during L-mode density ramp experiments in JET-Carbon (JET-C) and JET-ITER-Like Wall (JETILW) with carbon (C) and beryllium/tungsten (Be/W) plasma-facing components (PFC) respectively but identical divertor geometry. These high triangularity discharges (see Fig.1), feature a vertical inner and horizontal outer divertor target and have the primary X-point close to the inner target (IT). Dedicated detachment characterization experiments in this configuration were performed with C PFC and then repeated in the first JET-ILW campaign with the Be wall and W divertor.

Emphasis in the current study has been on matching as closely as possible the experimental conditions, given that the detachment characterization experiments were performed explicitly to gather the best possible data for modelling purposes.

With near-UV spectroscopy measurements, it has been possible to confirm experimentally the low target electron temperatures (Te) obtained by the code during the detachment process. The choice of the set of atomic physics processes accounted for in EIRENE [2,3] appears to be a key ingredient for the occurrence of the detachment in the EDGE2D-EIRENE simulations. Comparison between EDGE2DEIRENE and SOLPS4.3 (the version of SOLPS used to date at the ITER Organization for all divertor simulations [7]) modelling of the JET C PFC detachment experiment has also been performed and is presented here. Encouragingly, the two codes yield similar detachment behavior.

2. EXPERIMENTAL DENSITY RAMPS IN JET-C AND JET-ILW

JET Pulse No's: 79315 and 82342 in high triangularity at I_p = 2MA, B_T = 3T and P_{heat} ~ 3MW total heating power (ohmic and neutral beam injection (NBI)) were respectively selected as the references for detachment modelling in JET-C with C divertor and JET-ILW with Be wall and W divertor. The fuel species was not the same in both experiments, with hydrogen (H) used as working gas in the JET-C case and deuterium (D) in the JET-ILW discharge. The isotopic effect of H and D was investigated in the simulations, and it appears that the maximum IT and outer target (OT) ion flux is ~15% smaller when D is involved because its higher mass makes it slower. Small but not significant differences between H and D have already been seen in experiments and simulations on JET [8]. The code simulations described here in any case take the fuel species entirely into account.

During both the JET-C and JET-ILW discharges, the majority gas fuelling was applied in the private flux region (PFR) of the divertor in both cases, to produce a controlled density ramp, driving the divertor plasma from low recycling through high recycling to strongly detached regimes. As shown in Fig.2, the line-averaged electron density increases from $\bar{n}_e = 2.5 \times 10^{19}$ m^{-3} to 4.2×10^{19} m^{-3} during the ramp in the Cwall experiment and from $\bar{n}_e = 3 \times 10^{19}$ m^{-3} to 5.5×10^{19} m^{-3} in the Be/W case. The total radiative power increases from $P_{rad,tot}$ = 0.6MW to 2.1MW in C and from Prad,tot = 1.5MW to 2.2MW in Be/W. The plasma effective charge, Z_{eff} ~ 1.3 in C and 1.2 in Be/W, remains roughly constant throughout the density ramp, rising only near the end of the discharges, just before the density limit disruption which occurs in both cases. The fuelling rate used to control the density varies from 2.2×10^{22} s^{-1} to 2.7×10^{22} s^{-1} in C and from 2×10^{22} s^{-1} to 4.7×10^{22} s^{-1} in Be/W.

These detachment studies are focused on the evolution of the downstream Scrape-Off Layer (SOL) conditions during the two density ramps described in Fig.2. They make use of the experimental signals provided by the diagnostics presented in Fig.3. Efforts were made in both cases to provide the optimum set of divertor and SOL diagnostic signals, in order to better constrain the code simulations. Since both experiments were performed with very similar parameters (magnetic configuration, Pheat, I_p, B_t) with the exception of the fuel species (H in JET-C versus D in JET-ILW – see above) and the

wall material, they will assist in the understanding of the impact of the plasma-facing materials on the detachment process as the isotope selection has little or no impact on this process.

3. EDGE2D-EIRENE CODE SETTINGS

The same simulation grid is used for the JET-C and JET-ILW cases (Fig.4) and is built from an EFIT magnetic equilibrium reconstruction at t = 20s, midway through the JET-C density ramp. Within experimental uncertainties, the equilibrium is identical during the ramp and is considered similar in both the JET-C and JET-ILW discharges (see Fig.1). The vessel wall at the top of the main chamber was modified slightly in building the simulation grid to accommodate a wider SOL in the 2D grid. As may be seen using the better diagnosed JET-C case (IR data for the OT) in Table 1, the agreement between experiment and simulation for the power balance is reasonable.

Following [2], the albedo (or neutral reflection coefficient) of the vessel wall is adjusted for each of the two wall material cases (C and Be/W) to match the fuelling levels in the simulation with those observed experimentally. The dynamic retention [9] through implantation in the vessel wall is a transient phenomenon acting like a pump during the discharge and can be responsible for the mismatch between active pumping and fuelling rates in experiment. The computed albedos (see Table 2) increase through the discharges, consistently with the saturation behavior of the narrow range implantation mechanism (the hydrogen isotope is outgassed after the discharge and the short-term retention released [10]). Mention has to be made that it is unusual to account for this effect in EDGE2D-EIRENE simulations but in experiment, the total target particle flux in strongly detached regime is similar to the fuelling rate, thus the latter may have an impact on the simulations in these very particular conditions. This will be discussed in Section 6 where more classical settings - not involving main chamber wall pumping - are used.

The divertor pumping rate is deduced from the Penning gauges in the pumping duct, assuming roughly a temperature of 300K for the sub-divertor region and a pumping speed of $150 m^1.s^{-1}$ for the divertor cryogenic pump. A fine adjustment of this parameter accounting for isotopic effects or the NBI rotary valve has not been considered here since the objective is just to reach a realistic level of fuelling in the simulation, closer to the experiment. In the simulations with C and Be impurities, the albedo of the inner and outer divertor corners, mimicking the cryogenic pumps, is set at a constant value of 0.82 (independently of the vessel wall albedo) to match the experimental pumping rate ($1.7 \times 10^{22} s^{-1}$) obtained at the highest upstream density in the JET-C ramp. The latter experiment is used as a reference for this since it provides the best pressure measurements and the end of the ramp corresponds to the highest divertor neutral pressure, which should be close to the value measured in the pumping duct by the Penning gauges.

Since the divertor geometry is the same in the JET-C and JET-ILW experiments, it has been assumed for simplification that the albedo of the divertor pump has not been affected by the wall material change-out. The gas injection in the code is introduced in the private flux region (the NBI is assumed not to contribute to the discharge fuelling), as in the experiments, and the density is controlled at the outer midplane (OMP) separatrix.

In the simulations with C and Be impurities, the 3MW input power is split equally between electrons and ions, poloidal drifts are not activated, the Bohm criterion is applied at the target (Mach number M = 1) and electron and ion flux limiters are respectively set at 0.2 and 10 [11]. In Section 8, the effect of a variation of the total input power above and below 3MW has also been studied. The sheath heat transmission coefficients for the electrons and the ions are fixed at $\gamma_e = 4.5$ and $\gamma_i = 2.5$ respectively, the density decay length at the grid outer edge is 1cm. The sensitivity to the latter parameter has been investigated and appears to have a small effect on the far SOL conditions. Since the bulk of the particle and heat flux is near the separatrix, the target conditions are mostly not affected.

The C impurity is released by physical and chemical sputtering with the latter estimated according to the Haasz/Davis formula [12] with an enhancement factor of 0.5 since the simulations can match rather well the evolution of experimental radiated power with these settings (see Section 4.5 below).

The code runs are performed without W, assuming that the W targets are entirely coated with Be via main chamber migration [13]. The Be impurity is released only by physical sputtering. More generally, in these low power L-mode discharges, the divertor plasma should always be cold enough ($T_e < 100$eV) for the W target source to be negligible.

Two different reference EIRENE sets of atomic physics reactions are used in this study: the first is the so-called NIMBUS-like set of reactions [6], the default invoked by EDGE2D-EIRENE when no other option is specified and the second corresponds to the Kotov-2008 model (see Table 3) used in [2,3], which includes more atomic physics processes and allowed the modelling of detachment in [14]. Five other intermediate sets of reactions made by simplification of the Kotov-2008 model have also been implemented to identify the key process(es) involved in the detachment shown by EDGE2D-EIRENE in [14]. In all cases, EIRENE follows 64,000 neutral particles to reduce the statistical noise at high density.

4. CODE-EXPERIMENT COMPARISON

The code-experiment comparison proceeds by first constraining the simulations to match the measured upstream electron density (n_e) and T_e profiles since, at least up to the point of high recycling, the divertor conditions are sensitively dependent on upstream parameters. Once the upstream match is obtained, detailed comparisons can be made with the key experimental measurements of target parameters and distributed quantities such as radiated power and recycling. The various subsections below consider separately each of these key quantities to explore the level of agreement obtained with the simulations.

4.1 UPSTREAM PROFILES

The evolution of the upstream T_e (hereafter referred to as T_u) profiles is obtained from HRTS measurements in both JET-C and JET-ILW density ramps. For the upstream n_e (n_u) profiles, the Li-beam diagnostic provides a higher spatial and temporal resolution in comparison with HRTS, but is available only for the JET-C discharge. Profiles are obtained every 50ms with the HRTS and

every 20ms with the Li-beam. The nu and Tu profiles shown in Fig.5 for the different environments are obtained by averaging the measurements over a time window of ± 100ms for the Li-beam and ± 200ms for the HRTS at three different time slices in the ramps:

- t = 19.3s, 19.7s and 20.1s in the JET-C density ramp,
- t = 13.5s, 14.0s and 26.4s in the JET-ILW density ramp.

The same time windows are used to calculate the standard deviation associated with each average value.

The separatrix position is estimated using the two-point model [15] according to the procedure in [16] to compute first Tu in the lowest density (low recycling) case. It appears that to provide a match between the analytic prediction and the experimental HRTS data, the separatrix derived from the magnetic reconstruction (EFIT), must be shifted towards the high field side by ~1cm in JET-C and by ~1.7cm in JET-ILW experiments. As in [17], these separatrix shifts have been applied to all upstream experimental profiles throughout both density ramps.

The shifted experimental nu and Tu profiles provided respectively by the Libeam and HRTS diagnostics (blue lines in Fig.3a) in JET-C and HRTS alone in JETILW, are matched in the simulations (Fig.5) by adjustment of radially constant crossfield diffusivities which do not vary during the density ramp. The perpendicular particle and heat diffusivities are fixed at $D_\perp = 0.5 m^2.s^{-1}$ and $\chi_\perp = 1.5 m^2.s^{-1}$ for all ions species in both cases. These parameters allow a reasonably good description of the profile evolution in both JET-C and JET-ILW. Only the two density measurements obtained in the SOL from HRTS in the JET-ILW experiment at the highest density are not well matched by the code. In JET-C and JET-ILW, the Tu profiles measured by HRTS look similar at each density thus it is assumed that these upstream matches are satisfactory for JET-C and JET-ILW cases.

The upstream separatrix density limit at the OMP appears to be well simulated, with the code not converging after 2.3×10^{19} m^{-3} and 2.7×10^{19} m^{-3} with H plasma with C impurities and D plasma with Be impurities respectively. Experimentally, the discharges disrupted at $n_{u,sep} \sim 2.1 \times 10^{19} \pm 0.3 m^{-3}$ (JET-C) and nu,sep ~ $2.7 \times 10^{19} \pm 0.4 m^{-3}$ (JET-ILW). The experimental upstream separatrix density limit is ~ 30% higher with metal walls than with C PFC, to be compared with ~20% difference between the two from the code simulations. This is one of the main differences between the JET-ILW and JET-C density ramps found in both experiment and simulations [17].

4.2 TARGET LANGMUIR PROBES

The divertor LP (magenta squares in Fig.3c) provide the main constraint for the code simulations at the divertor targets. Interpretation of the probe data is not straightforward under high recycling and strongly detached conditions. Visual inspection of the current-voltage (I-V) characteristics from single probes reveals that the ion current often fails to saturate, instead increasing continuously with decreasing voltage. This behavior can be explained by the expansion of the electrostatic sheath into the plasma around the probe, and is often observed on tokamak LP characteristics [18]. This

is also the case here, especially for the low temperature measurements (see example in Fig.6a). Neglecting sheath expansion effects can lead to large errors in the T_e derived from the probe characteristics [19].

To account for sheath expansion, for the purposes of this article, the probe data are mostly processed with a 4-parameter fit method. In a few cases, especially when T_e is high (making it difficult to clearly separate the ion current due to sheath expansion from the electron current), the 4-parameter fit gives spurious results and a standard 3-parameter fit is preferred (Fig.6b). The 3 and 4-parameter fits are performed according to the following formulas:

$$I = I_{sat}(1 - e^{\frac{V-V_f}{T_e}}) \text{ ; 3-parameter fit} \quad (1)$$

$$I = I_{sat}(1 - e^{\frac{V-V_f}{T_e}}) + \frac{dI}{dV}(V - V_f); \text{ 4-parameter fit} \quad (2)$$

with the probe current I and the ion saturation current I_{sat} in A, the probe voltage V and the floating potential V_f in V, T_e in eV and the slope dI/dV in AV^{-1}. In what follows, the ion saturation current density J_{sat} is calculated by dividing the value of the fitted ion current I_{sat} by the geometrical projection of the probe surface area along the magnetic field lines.

This treatment of the single probes raw data is applied over 5ms sweeps in voltage in both cases from 19.25s to 20.25s in C and from 13.3s to 16.5s in Be/W (see Fig.2 for the timing in each discharge). Each value of Jsat or Te is obtained by averaging over a time window of ± 50ms in JET-C and ± 20ms in JET-ILW. A standard deviation is also calculated over the same time windows and associated with each average value. As shown in Fig.7, for each LP, 4 values of T_e and J_{sat} have been selected at the time slices defined in Fig.2 in the JET-C and JET-ILW ramp. Inspection of the OT J_{sat} time dependent profile in both discharges, confirms that the four time slices correspond approximately to:

- a low recycling regime (green) at the beginning of the density ramp where the OT particle flux is still increasing,
- a high recycling regime (black) when the OT particle flux time dependent profile reaches its maximum,
- a partially detached regime (blue) when the OT particle flux start to decrease while the n_u is still increasing,
- a strongly detached regime (red) when the OT particle flux reaches is minimum and n_u reaches its maximum.

The error on the values of nu at each chosen density comes from an uncertainty of ± 1cm on the separatrix position given by the method described in [16].

Although the OT J_{sat} measurements can be associated with a clear detachment process, the

situation is much less obvious on the IT where only one or two probes are located in the SOL and measure significant Jsat values. Qualitatively, a reduction in the particle flux with increasing nu can be seen on the limited available measurements for both the JET-C and JET-ILW discharges. There is also evidence for an in-out divertor particle flux asymmetry, with earlier detachment at the IT. According to the simulated profiles in Fig. 7, the bulk of the profile seems to be on the upper inner baffle and is not observed due to the absence of probes in this region. This is consistent with the large inner poloidal flux expansion (see Fig.3c).

As shown in Fig. 7, where the simulated and OT and IT LP data are compiled at the four different times of the density ramps identified in Fig.2, the trends of the observed divertor detachment are essentially similar for both JET-C and JET-ILW experiments. Since in both discharges, the divertor passes through low recycling, high recycling, partially detached and strongly detached regimes, there is a good scope for code-experiment comparison. Simulations with the Kotov-2008 neutral model provide reasonable agreement with the magnitude (less than 30% discrepancy at the OT), and especially the trend of the target particle flux evolution. However, the lack of probes on the IT does not allow the level of analysis possible for the OT. Only for the Kotov- 2008 model do the code simulations reproduce clearly the experimentally observed profile of particle flux detachment at the OT.

Even if the experimental target T_e profile is well reproduced by the code for the OT in the low recycling case, most of the experimental target Te values do not show the collapse obtained by the simulation for the high recycling, partially detached and strongly detached phases even though, as discussed above, the OT particle flux is matched to better than 30% discrepancy. At the IT, only the LP Te for the JET-ILW low recycling case is reproduced by the simulation (within the small range of profile for which data are available).

The in–out asymmetry, with an earlier detachment at the IT seen for both JETILW and JET-C experimental cases is challenging to reproduce in this type of simulations, even with drift terms activated [3]. A modelling attempt with EDGE2DEIRENE is presented in Section 8, showing that the observed asymmetric detachment can be at least qualitatively reproduced by the code if an asymmetric distribution of power entering the divertor is assumed.

As shown in [20], the polarization and the friction occurring when current flows through the plasma surrounding the LP could also significantly affect the T_e measurements in high density, low temperature plasma. Since, in these conditions, ion current circulates over less than a few millimeters through the highly resistive target plasma to close the circuit between each probe and the wall, large cross-field currents are expected, generating j×B forces which must be counteracted mainly by friction with neutrals or by a polarization drift [20]. Consequently, a higher voltage is required to reach ion saturation, which leads to an overestimation of Te when fitting the I-V characteristic. In the ranges of T_e (from ~ 1eV to ~ 20eV) and n_e (from ~10^{19} m^{-3} to ~10^{20} m^{-3}) explored during the experimental density ramps presented here, the analysis in [20] would conclude that the polarization effects are dominant.

As an example, in partially detached and strongly detached conditions in JET with $n_e \sim 10^{20}\,m^{-3}$ and $T_e \sim 1eV$, [20] suggests that polarization effects alone could drive the maxima of the T_e probe measurements nearly 4 times higher than the real local values. Similarly, in high recycling conditions in JET, with $n_e \sim 10^{20}\,m^{-3}$ and $T_e \sim 5–10eV$, the maximum of the Te probe measurements could be between 1.3 and 2 times higher than it may be in reality. In attached conditions with $n_e \sim 10^{19}\,m^{-3}$ and $T_e > 10eV$, the polarization effects would not be expected to affect the T_e measurement. This is consistent with the fact that experiments and simulations compare reasonably well in this regime at the OT in both the JET-C and JET-ILW discharges. Of course, the polarization effect does not exclude the simultaneous presence of other effects, so that the measured T_e may exceed the right value by even stronger factors than governed by polarization alone. Similar analysis at the IT is prevented both by the lack and poor quality of data in this region of the divertor.

Assuming that polarization effects play a role would bring significant portions of the experimental T_e profiles to values of ~ 1eV in JET-C for the partially detached and strongly detached phases. It is worth noting that in JET-ILW, during the same phases, some T_e measurements near the strike point are already very low without any corrections for some reasons which are not yet clear. Thus, the subtraction of the polarization effect in these cases could bring the experimental Te profiles to even lower values. In both environments, it would be more consistent with EDGE2DEIRENE simulations. As shown in Fig.8, in these conditions, a significant volume recombination source appears in the simulated plasma and can be identified in the experiments (see Section 4.7), which is consistent with low T_e in the divertor. The difference between total ionization and recombination rates is similar with both neutral models in the first part of the simulated ramps with C and Be impurities, but with the NIMBUS-like neutral model, the run stops at lower nu, while with the Kotov 2008 neutral model, it reaches lower temperature where the volume recombination becomes stronger, reducing the particle source in the last part of the ramps. It appears that the detachment modelled by the code in both environments occurs mainly at this stage which would be consistent with [21].

The difficulties of measuring Te precisely when the plasma is not attached to the targets, in both JET-C and JET-ILW discharges, lead to large uncertainties in the deduced values of n_e and perpendicular heat flux density ($q_\perp$). Thus, the significant discrepancies between experiment and simulation for both wall materials in Figs.7 and 9 are expected independently of the atomic physics model used in EIRENE.

Even if in JET-ILW the inner and outer strike point T_e measurements are already more consistent with the code without subtracting the polarization effect, the bulk of the T_e target profiles is still much higher than in the simulations in high recycling and beyond, as in JET-C. Any overestimation of T_e obtained from the probes leads to underestimation of ne and overestimation of $q_\perp$. For the latter in particular, the uncertainty on the value of the sheath transmission coefficients for the electrons and the ions [22] (respectively $\gamma_e = 4.5$ and $\gamma_i = 2.5$ assumed here) adds another source of possible error. However, since the experimental OT profiles of J_{sat} and T_e are well matched by the simulations in the attached phases for JET-C and JETILW, the densities are also well simulated by

the code in these cases. Even if the experimental OT densities do not reach the simulated values (factor 3 discrepancy for the partially detached and strongly detached regimes), the experimental trend showing a decrease of ne in the strongly detached regime is qualitatively reproduced by the code and a strong reduction of $q_\perp$ can also be noted in both experiments and simulations.

One can note that the T_e values obtained from the polarization argument presented earlier would bring the experimental n_e and $q_\perp$ profiles in the high recycling, partially detached and detached phases closer to the simulation results.

4.3 INFRARED DEDUCED POWER LOAD PROFILES AT THE OT

High resolution IR thermography (see Fig.1), is available for measurement of the OT $q_\perp$ profile in the JET-C experiment. In this case, the uncertainties inherent in the computed LP power flux density profile are absent. The comparison between the IR data and the simulated values for $q_\perp$ in the four different phases of the JET-C density ramp is shown in Fig.10. As seen earlier in the comparison with LP data, only the Kotov-2008 model is capable of reproducing the low heat flux reaching the target in the strongly detached regime.

Experiment and simulation both show a strong decrease of $q_\perp$ with increasing upstream density, but are in significant disaccord (up to factor 3 - 4) for the high recycling, partially detached and strongly detached phases. The thermography derived $q_\perp$ contains neutral and photonic power density deposition contributions on the target in addition to the plasma fluxes and the camera also collects parasitic signals due to reflections from the vessel walls. In contrast, in the simulation, $q_\perp$ is due only to the plasma contribution. For the JET-C density ramp, reflections are expected to be limited and the main source of differences between simulation and measurement is assumed to come from the neutral and radiative power load on the OT.

As shown in Fig.11a, the averaged experimental PFR $q_\perp$ (shaded band in Fig.10) increases through the density ramp, at the same time as the OT heat flux density decreases strongly. Since the plasma heat flux density is expected to be negligible at this location in the PFR, non-zero power deposition can come only from the OT neutral and radiative power load. This PFR heat flux density background has been subtracted from the original IR data to give the reprocessed OT profiles shown in Fig.11b. The agreement between code and experiment is now much better in magnitude. However, the maxima of the experimental and simulated profiles move in opposite directions with increasing nu, for reasons which are not yet understood. This effect could be related to the calibration of the diagnostic or also a possible decoupling between the particle flux and the heat flux. Further work would be required on this topic to have an answer.

If the sheath heat transmission coefficients are assumed to remain more or less constant during the ramp [22], the good match in absolute magnitude between the corrected IR data and the code indicates that the experimental target T_e should indeed collapse much faster than indicated by the LP, as in the simulations. This would be another indication of the presence of low T_e and hence a significant volume recombination source during the experimental partially and strongly detached phases.

4.4 EXPERIMENTAL AND SIMULATED PRESSURE DROP IN DIVERTOR

As explained in [23], the reduction of divertor plasma pressure compared to upstream - while the target T_e is decreasing - is an indicator of detachment. The LP n_e and T_e obtained for the two Pulse No's: 79315 (JET-C) and 82342 (JET-ILW) around the inner and outer strike points can be used to calculate the divertor plasma pressure, which may then be compared to the OMP separatrix plasma pressure obtained from the ne and Te measured by the Li-Beam and HRTS in JET-C and HRTS only in JETILW. The pressure drop factor fmom, is given by the ratio of the downstream to upstream pressure according to [23]:

$$f_{mom} = \frac{2 n_t T_t}{n_u T_u} \tag{3}$$

with n_t and T_t representing the target density and temperature, respectively.

The upstream and downstream impurity concentrations are assumed sufficiently low that $n_e \approx n_i$ and the collisionality sufficiently high for $T_e \approx T_i$. In fact, the code simulations verify these assumptions within a reasonable margin. Even at the lowest nu, $T_{ui}/T_{ue} \sim 1.2$ and $T_{te} = T_{ti}$. The objective is to compare these experimental inner and outer divertor pressure drop obtained in both C and Be/W at the strike points with simple atomic physics trends and the EDGE2D-EIRENE simulations with C and Be impurities. The results of this exercise are compiled in Fig.12.

The analysis of Self and Ewald [24] considers that the divertor pressure drop associated with the detachment is related to the neutral-ion collisions which decrease the target ionization source by slowing down the recycling neutrals. According to [23], it has the following trend:

$$f_{mom}^{cx} = 2\left(\frac{\alpha}{\alpha+1}\right)^{\frac{\alpha+1}{2}} \text{ with } \alpha = \frac{\langle \sigma v \rangle_i}{\langle \sigma v \rangle_i + \langle \sigma v \rangle_{cx}} \tag{4}$$

with $\langle \sigma v \rangle_i$ and $\langle \sigma v \rangle_{cx}$ respectively the ionization and charge-exchange rates for a pure hydrogenic plasma (see e.g. [25]).

As described in [23], the 2-point model accounting for radiative power losses and target pressure losses (according to (4)), is based on the following system of relations between upstream and downstream:

$$2 n_t T_t = f_{mom}^{cx} n_u T_u \tag{5}$$

$$T_u^{7/2} = T_t^{7/2} + \frac{7}{2}\frac{q_{//} L}{\kappa_{0e}} \tag{6}$$

$$\begin{gathered} q_{//} - \frac{14}{3} L c_z n_u^2 L_z = \gamma n_t e T_t c_{st} \\ \text{with } q_{//} = \frac{P_{heat} - P_{rad\_core}}{4\pi R \lambda_q \theta_{pitch}},\ \theta_{pitch} \approx \frac{2\times 10^{-7} I_p}{a B_t} \text{ and } c_{st} = \sqrt{\frac{2eT_t}{m_i}} \end{gathered} \tag{7}$$

All the constants with their units applied in the particular case studied here are described in Table 4 below.

Now, if a volume recombination source (with the rate $<\sigma v>_{rec}$ from [25]) is considered over a given distance L_{rec} in the parallel direction from the target is taken into account, a new target density n_{trec} is obtained, such as:

$$n_t c_{st} - n_{trec}^2 \left\langle \sigma v \right\rangle_{rec} \left(T_t \right) L_{rec} = n_{trec} c_{st} \tag{8}$$

In this case, the target particle source would be decreased by the increase of volume recombination and the associated pressure loss $f_{\mathrm{mom}}^{\mathrm{rec}}$ (instead of $f_{\mathrm{mom}}^{\mathrm{cx}}$) can be calculated here with the parameters given in Table 4 such as:

$$f_{mom}^{rec} = \frac{n_{trec}}{n_t} \tag{9}$$

At first sight, on Fig.12, the experimental pressure loss at the inner and outer strike points in JET-C seems to be closer to $f_{\mathrm{mom}}^{\mathrm{cx}}$ while in JET-ILW, it is between $f_{\mathrm{mom}}^{\mathrm{cx}}$ and $f_{\mathrm{mom}}^{\mathrm{rec}}$. However, as discussed in Section 4.2 and 4.3 above, the target T_e given by the LPs is significantly overestimated and the polarization drift effect has not been subtracted in Fig.12. Thus, even if the T_e measurements near the strike points in JETILW are already quite low, the experimental pressure values must be translated to lower T_e values, in the direction of $f_{\mathrm{mom}}^{\mathrm{rec}}$. Consequently, in JET-ILW at least, the target T_e is likely to be very low when the plasma has essentially detached. One can actually note that most of the IT experimental data is accumulated during this phase in both environments which means that, as often observed in tokamaks, the IT detaches sooner than the OT. Mention has to be made that a reasonable uncertainty of ± 1cm on the position of the separatrix found in Section 4.1 would add a margin of ± 50–60% to the experimental fmom values on Fig.12.

These results can be compared with the pressure drop factors obtained from (3) using the much more complex EDGE2D-EIRENE model (Fig.12) accounting for the wall geometry, the magnetic equilibrium, volumetric effects (particle sources, radiative power losses, momentum sources) and an advanced set of atomic physics processes (Kotov-2008 model in Table 3). In both simulations with C and Be impurities, the decrease of pressure at the IT strike point begins below 1-2eV and evolves in the range of very low T_e, like $f_{\mathrm{mom}}^{\mathrm{rec}}$. At the OT strike point, the pressure drop begins at higher T_e, closer to the values characteristic of $f_{\mathrm{mom}}^{\mathrm{cx}}$, but requires lower T_e to become stronger and eventually becomes similar to the IT strike point pressure drop. Thus, on both targets and in both environments, the EDGE2D-EIRENE simulated pressure drop requires very low T_e values (≤ 1eV) at the strike point compatible with the strong volume recombination source of Fig.8, which is consistent with [21].

The experimentally observed in-out asymmetry in the detachment process with an accumulation of low pressure values correlating with low T_e on the IT is not reproduced in the simulation. This

topic will be discussed with more details in Section 8. It is also worth noting that the simulations show the same maximum divertor pressure drop as in experiment, namely ~1 and ~2 orders of magnitude at the OT and IT strike points respectively for both JET-C and JET-ILW. According to the code and the experiment, this difference can be attributed to a significantly lower strike point T_e on the IT than on the OT (see Fig.7).

The simulated partially detached and strongly detached phases with C and Be impurities show a much stronger ionization source in the inner divertor compared with the outer (see Fig.13). This can be attributed to the vertical versus horizontal target geometry: recycling neutrals from the inner vertical target encounter an increasing temperature gradient and are re-ionized more efficiently than in the outer divertor, where they recycle from a horizontal target, crossing a decreasing temperature gradient and with a higher probability of escaping the plasma. The significantly higher power losses, due to the ionization processes, in the inner divertor compared with the outer one, decrease the T_e more efficiently at the IT than at the OT.

4.5 RADIATIVE POWER DISTRIBUTION

In both JET-C and JET-ILW density ramp experiments, the total radiative power, coming mainly from H or D atoms and C or Be impurity species, is measured with the two sets of bolometric chords in the horizontal and vertical direction (see Fig.3b). The horizontal and vertical chord measurements for the usual four chosen upstream densities are compared to the EDGE2D-EIRENE simulation results (obtained with the Kotov-2008 atomic physics model of Table 3) processed with an equivalent synthetic diagnostic, in Fig.14 for the JET-C and JET-ILW discharges.

In the case with C impurities, simulated values show a remarkably good agreement with the horizontal bolometric signals at each upstream density and for the majority of the chords (see Fig.14a,b). Only the radiative power coming from the chords between 140 and 160 degrees is underestimated in the simulation by a factor up to 2–3 compared with the experimental measurements. This range of LOS corresponds to the upper part of the machine not well modelled by EDGE2D-EIRENE. The void between the wall and the fluid domain of the simulation is in reality filled with the far SOL plasma which is mainly connected to the divertor baffles and the upper dump plates where it recycles and generates radiating C impurities.

The code results also reproduce quite well the experimental measurements along the vertical chords between 235 and 275 degrees and tend to overestimate the radiative power coming from the low field and high field sides of the main chamber wall. Since the simulation does not account for the far SOL, in the main chamber the recycling and impurity generation occurs on the low and high field sides of the wall and the radiative power is produced in this region instead of the divertor baffle and the upper dump plates. This is actually consistent with the above mentioned underestimation of the radiated power found by the code in the secondary X-point region at the top of the main chamber.

However, in both JET-C experiment and code, the main source of radiative power is found to be

in the divertor and the measured and simulated evolution of its magnitude with nu is very similar (less than 20% difference).

In JET-ILW, the discrepancies between experimental horizontal and vertical chord measurements and EDGE2D-EIRENE simulation results are more significant (see Fig.14c,d). The position of the main source of radiative power in experiment is reproduced by the code, but the evolution of its magnitude with nu is not very well modelled. The simulations tend to underestimate the radiated power by a factor ~ 2 compared to experiment for the divertor source and up to an order of magnitude for the rest of the plasma.

Tungsten core radiation is known to be significant under some conditions in ILW plasmas [26]. Since the EDGE2D-EIRENE simulations with Be impurities do not include W and do not model the core, they miss this possible radiative power contribution which could be the reason for the mismatch with the experimental chord measurements for the JET-ILW experiment.

The distribution of radiation in the plasma is the other main difference between the JET-C and JET-ILW discharges [26]. As shown in Table 5, the fraction of the input power radiated in the divertor and throughout the whole plasma is more important in JET-ILW than in JET-C at the beginning of the ramp. In contrast, at the highest densities, the divertor and total radiation fraction are higher in JET-C than in JET-ILW. This is why the density limit is higher in JET-ILW [17].

In all cases, the core radiated power is higher in JET-ILW than in the JET-C experiment and this difference can reach a factor ~2 at low density. With C impurities, the total power radiated from the EDGE2D-EIRENE simulation domain matches the experimental divertor radiative power within < 20% when the Haasz/Davis formula [12] with an enhancement factor of 0.5 is involved for the chemical sputtering of C. For the JET-ILW discharge, the experimental divertor radiated power is ~2 times stronger than the code value at low density and 25% higher than in the simulation at high density.

As shown in Table 5, in the simulations with C impurities (which is a powerful radiator at low SOL/divertor temperatures), the radiated power from carbon is always ~3 times higher than that from hydrogen, while in the simulations with Be impurities, the Be and D radiated powers are always similar in magnitude, confirming that Be is a poor radiator in the SOL.

Even if in the simulations for the JET-ILW experiment it is assumed that the divertor is entirely coated with Be, the simulated radiated power is insufficient to retrieve the divertor measurements. This means that in the JET-ILW experiment analyzed here, one or several other sources of radiation are involved. Simulations with two impurities, Be and W, have already shown (see [17] and [27]) that W is not responsible for this missing contribution in the divertor. However, W could be responsible for the enhanced core radiative source seen on Fig.14c which would add to the experimental data from the vertical bolometry viewing the divertor.

It is known from [28] and has been verified in the JET-ILW Pulse No: 82342 examined in this paper, that the concentration of C is at least an order of magnitude lower than in the equivalent JET-C experiments. Assuming that the residual C impurity in the JET-ILW discharge radiates

with a similar distribution to that observed with the carbon PFC, but a factor 10 lower in absolute power, it would add a maximum contribution of ~0.04MW to the simulated impurity radiation at the beginning of the ramp and ~0.11MW at the end. This would increase the radiative fraction from 13% to 15% at the beginning of the ramp and from 29% to 33% at the end in the simulations. This is still insufficient to reach the experimental divertor radiative fractions of 26% and 40% for the beginning and end of the ramp respectively.

The divertor spectroscopic chord measurements (Fig.3a) show an order of magnitude increase in the intensity of O+ and N+ line radiation in the JET-ILW discharge compared with the JET-C discharge. Both impurities are known to be excellent radiators in the SOL and oxygen reaches its maximum cooling rate when T_e is between 10eV and 20eV [29], corresponding to the attached conditions of the JET-ILW experiment where the radiative contribution missed by the simulation is largest. EDGE2D-EIRENE simulations including selectively O and N impurities along with Be would be required to verify this speculation. There is also the possibility that the fraction of the radiative power due to H or D is higher in experiments than in simulations. Nevertheless, it is important to reiterate that the simulations described here for the C dominated experiment do provide an excellent match with the experimentally measured line integral radiation distribution.

4.6 TOMOGRAPHY COMPARED TO EDGE2D-EIRENE SIMULATION RESULTS

Tomographic reconstructions obtained from the bolometry measurements are compared in Fig.15 to the EDGE2D-EIRENE simulation results (obtained with the Kotov-2008 model of Table 3) at the beginning and the end of the density ramp for the JET-C and JET-ILW cases. The good match obtained for the bolometric LOS in the JET-C discharge is not found with the tomography, casting a serious doubt regarding the uniqueness of the reconstruction. For both the JET-C and JET-ILW discharges, the tomography always tends to show the radiation sources concentrated around the X-point while the code places the radiative power at the IT and the OT at low upstream density and spreads it over a more extended region between the IT and the X-point at the end of the ramp.

In simulations, during the strongly detached phases with C and Be impurities (Fig.16) the IT radiated power source is mainly due to H (in C) or D (in Be) and the X-point source is essentially due to impurity radiation. This IT source is related to the strong recycling mentioned in Section 4.4 and shown in Fig.13. When the divertor plasma is strongly detached, a volume integration performed over the radiating cells above the X-point gives 0.5 MW in the simulation with C and 0.2MW in the simulation with Be. The same calculation for experimental tomographic reconstructions, yields 0.6MW in JET-C and 0.2MW in JET-ILW. At this density regime, and for this particular region of the plasma, the tomography seems to be reasonable but it systematically misses the radiated power sources at the targets, at least in the cases presented here.

In the simulations, C and Be impurities are produced by sputtering (physical and chemical for C and physical only for Be) mainly at the IT and OT strike points, where the particle fluxes are the highest. The distributions of the most relevant Be and C impurity species in the divertor are shown

in Figs.17 and 18 respectively for the simulated strongly detached phase of Fig.16.

In both simulations, the neutral C^0 or Be^0 impurities are ionized close to the targets producing the main respective divertor impurity species: C^+ and Be^+. Be^0 is ionized faster than C0 because of a lower ionization energy threshold. At both IT and OT, when the divertor plasma is strongly detached, the small parallel temperature gradient along the separatrix (mainly cooled by the radiated power) coupled with the significant C^+ or Be+ parallel density gradient generates a strong parallel pressure and viscosity gradient which pushes these impurities away from the targets in the direction of the X-point. Near the latter, the density gradient between the SOL cells and the neighboring core cells drives the C^+ and Be^+ impurities across the separatrix by diffusive perpendicular transport. The higher temperature in the core cells above the X-point allows the ionization of a significant fraction of Be+ to Be^{2+} giving a mix of both species (Fig.17) responsible for the radiation distribution seen in this region in the simulations with Be impurities (Fig.16).

The high simulated densities of Be^{2+} on the inner baffle from main chamber sputtering could explain the Be deposition found by recent post-mortem analysis of JET-ILW inner divertor tiles [30]. However, this study also revealed that Be was absent on most of the other divertor surfaces (the OT in particular) which means that the Be content in the simulations is probably overestimated.

In the simulations with C impurities, two successive ionization steps in the core cells give a mix of C^{2+} and C^{3+} (Fig.18) responsible for the radiative power source seen above the X-point (Fig.16). In both simulations with C and Be impurities, the IT seems to contribute more than the OT to this source.

4.7 EXPERIMENTAL AND SIMULATED VOLUME RECOMBINATION

Near-UV spectroscopy was available in both JET-C and JET-ILW discharges for the OT (see Fig.3.4b) and gives access to high-n Balmer series line radiation [31]. The analysis here concentrates on the evolution of the OT profiles for the 11 to 2 transition, recognizing that a high-n line intensity would be an experimental signature of a high volume recombination rate. The time window for the calculation of the average values and the standard deviations of the profiles shown in Fig.19 is ± 40ms.

In Fig.19, these measurements for the four chosen upstream densities are compared to the EDGE2D-EIRENE simulation results (obtained with the NIMBUSlike and Kotov-2008 atomic physics model of Table 3), processed with an equivalent synthetic diagnostic, for the C and Be/W discharges respectively.

In both cases, the experimental trend is reproduced by the code with around two orders of magnitude increase of the 11-2 line intensity profile between the beginning and the end of the density ramps. The highest intensity, corresponding to the highest rate of volume recombination (Fig.8) in the strongly detached phase is found only by the simulation made with the Kotov-2008 model. The experimental and simulated data are closer on the outboard side of the OT. On the inboard side, the experimental intensities are much higher than in simulations. This would come from a strong recombination source present in experiment in the X-point region but not reproduced by the code.

This also means that the simulations underestimate the H or D radiative power in this region.

Since most of the experimental values are above the simulation results and that $T_e \leq 1$eV is required on the OT to reach the volume recombination rate associated with the partially and strongly detached cases, the implication is that $T_e \leq 1$eV in experiment during the same phases. Since the volume recombination seems in fact to be usually stronger in experiment, the real experimental T_e may be even lower than in the simulations. This is another evidence that the T_e obtained from the LP by a 3 or 4–parameter fit during the detachment are overestimated and that the low simulated values are actually closer to reality as already indicated by the comparison between code result and IR measurements in Section 4.3.

4.8 D_α-H_α, C^{2+} AND BE+ LINE RADIATION DISTRIBUTION

As shown in Fig. 3a, four spectroscopic LOS collect the D_α-H_α, C^{2+} and Be^+ line radiation from different regions of the plasma. The intensity of the H_α and D_α lines from the JET-C and the JET-ILW experiments respectively are matched by the EDGE2D-EIRENE simulation results (obtained with the Kotov-2008 atomic physics model of Table 3) mostly within a factor 2–3 (see Fig.20). Only the 3rd density point is nearly an order of magnitude lower than measured in both cases and there is no clear explanation for this. It is already shown with the LP in Section 4.2 that the agreement between code and experiment is reasonable at the OT in both environments.

According to Fig.21, the experimental distribution of C^{2+} is matched within a factor ~2 by the code, with the exception of the low recycling phase in the inner and outer divertors where the simulations overestimate the C^{2+} line radiation intensity by a factor 3–4. One could expect a better match since, in the JET-C case, the agreement between code and bolometric LOS measurements is remarkably good (see Section 4.5). However, the radiative power measured by the bolometry is essentially due to C^{3+} while the spectroscopy is sensitive to C^{2+} lines. This could mean that the distribution of C^{3+} is better matched by the code than the distribution of C^{2+} In the Be/W discharge, the experimental distribution of Be^+ during the high recycling, partially detached and strongly detached phases in the outer divertor is matched within a factor 2–3 by the simulations with Be impurities but the discrepancies range from factors of ~4 to 10 for the other LOS. In all cases, the code overestimates the Be^+ line radiation intensity compared to experiment, indicating that the W divertor targets are probably not fully coated with Be as assumed here. This is consistent with very recent experimental evidence from post-mortem analysis of JETILW divertor tiles extracted following the first campaign [30].

However, even if the concentration of Be impurities is overestimated by the code, the latter underestimates the radiated power, confirming the suspicion (mentioned in Section 4.5) that one or several other sources of radiation are involved in the JET-ILW experiment (remaining radiative impurities, stronger contribution from D, and/or stronger contribution from the core).

5. ATOMIC PHYSICS AND DETACHMENT IN EDGE2D-EIRENE SIMULATIONS

Most of the simulation results presented in the previous sections were obtained with the Kotov-2008

model with which detachment signatures are more clearly obtained in EDGE2D-EIRENE [14]. As mentioned in Section 3, several intermediate EIRENE atomic physics models lying between the NIMBUS-like and Kotov-2008 descriptions (see Table 3) have been tried to identify the atomic physics process, or combination of processes allowing the detachment obtained in the EDGE2D-EIRENE simulations. These intermediate models are constructed by simplification of the Kotov-2008 model as follows:

(a) Kotov-2008 without the CRM
(b) Kotov-2008 without the elastic and inelastic molecule-ion collisions
(c) Model (b) without the H^{2+} ions
(d) Kotov-2008 without the elastic molecule-ion collisions
(e) Kotov-2008 without the inelastic molecule-ion collisions

In Figs. 22 and 23, the total target particle and heat fluxes given by EDGE2DEIRENE runs with the models (a-c) and (d), (e) respectively with C impurities are compared to those obtained with the NIMBUS-like and Kotov-2008 models. It is clear that the absence of elastic and inelastic collisions between ions and molecules is the only option preventing particle flux detachment in the simulation. Similar target heat flux removal is obtained in all cases. Fig.23 demonstrates that the strongest particle flux reduction requires the involvement of elastic molecule-ion collisions. When this process alone is accounted for, the integrated target ion current is reduced by a factor 3–4 from the highest value at the rollover and to the lowest value at the highest n_u. The importance of this process is in agreement with the analysis performed in [32] for detachment modelled by SOLPS.

As shown in [33], for $T_e < 5$eV, the reaction rates given by the CRM for the reactions (11), (5) and (6) in Table 3 (including the production of H_2^+ ions) and the rate of inelastic molecule-ion collisions become negligible compared to the rate of elastic molecule-ion collisions. The rates for these reactions is at least one order of magnitude above those for the other processes and dominates the atomic physics of the detachment modelled by EDGE2D-EIRENE when the Kotov-2008 model is invoked.

It is important to note that the target T_e threshold, set at 1eV in EIRENE and allowing the recycling to switch from atomic to molecular, is a key parameter to trigger the massive production of molecules required for the elastic molecule-ion collisions to become significant. However, this value, chosen here as fixed independently of wall material, is somewhat arbitrary since in reality, the switch from atomic to molecular recycling is probably a smooth process starting at $T_e > 1$eV and strongly material-dependent [34,35]. Since the rate of the elastic molecule-ion collisions does not change much with T_e [33], a higher T_e threshold may have an impact on the modelling of the detachment.

6. EDGE2D-EIRENE/SOLPS4.3 COMPARISON

SOLPS4.3 is the basic physics code used to model the ITER divertor, the design of which has been strongly guided by the simulation results (see for example [36]). Here we attempt a partial code

validation study, in which the detachment obtained with the SOLPS4.3 and EDGE2D-EIRENE codes is compared for the JET model with C impurities.

To facilitate the comparison, the model is simplified in the same way in both SOLPS4.3 and EDGE2D-EIRENE. The aim is not to obtain quantitative agreement with the experiment, which requires fine adjustment of the model parameters, but to reproduce the experimental trends, already seen in the EDGE2D-EIRENE simulations, with SOLPS4.3. In this study, only the inner and outer corner surfaces of the divertor are pumping, with a constant albedo of 95%. The original grid corresponding to the EFIT equilibrium of Pulse No: 79315 (the JET-C discharge) at 20s is used in EDGE2DEIRENE and SOLPS4.3 without the modification of the upper regions of the vacuum vessel (no extended grid). The chemical sputtering yield for C is set constant at 1% everywhere. Finally, the radial transport and the boundary conditions are set as in Section 2.

In Fig.24, the results from EDGE2D-EIRENE and SOLPS4.3 simulations with both NIMBUS-like and Kotov-2008 neutral models are compared at the target positions corresponding to individual probes near the inner and outer strike points (see Fig.25). Both codes show a significant and similar drop of the plasma heat flux on the targets with increasing nu for both atomic physics models. On the IT, when the NIMBUS-like model is employed, the Jsat given by SOLPS4.3 continues to increase, while EDGE2D-EIRENE result first saturates and then decreases slightly. With this neutral model, the upstream density limit (at which the code is not stable anymore) is found to be essentially the same in both codes (1.8×10^{19} m^{-3} for SOLPS4.3 and 2×10^{19} m^{-3} for EDGE2D-EIRENE).

For both codes, the use of the Kotov-2008 model in EIRENE leads to a decrease of the Jsat on the IT after the roll-over. However, the decrease is significantly stronger with EDGE2D-EIRENE than with SOLPS4.3, where stable code runs are possible only up to $n_u = 1.9\times10^{19}$ m^{-3}, compared with $n_u = 2.2\times10^{19}$ m^{-3} for EDGE2D-EIRENE. On the OT, SOLPS4.3 and EDGE2D-EIRENE both show a maximum followed by a decrease of Jsat with the NIMBUS-like model and a more pronounced drop (for EDGE2D-EIRENE in particular) for Kotov-2008. The difference between the results from the two neutral models is not as strong in SOLPS4.3 as in EGDE2D-EIRENE, but it is noticeable. It can be noted that the simplified setting used here for the pumping surfaces - compared to the more complex one presented in Section 3 - does not affect strongly the simulated detachment behavior.

Before the rollover, for both IT and OT, the particle flux density from SOLPS4.3 is always lower than from the EDGE2D-EIRENE, but the rollover occurs at about the same n_u ($1.5\times10^{19} - 1.7\times10^{19}$ m^{-3}) in both codes. At the rollover and beyond in the ramp, the simulated particle flux densities are much closer no matter which neutral model is invoked. The reason for the difference in Jsat at lower n_u is still unclear, but similar behavior was reported from a comparison between SOLPS4.3 and SOLPS5.0 in [37].

This particular study shows that the experimental trends around the J_{sat} rollover, reproduced by EDGE2D-EIRENE for JET-C high triangularity L-mode density ramps, are also seen in the SOLPS4.3 results obtained with similar settings.

7. DIVERTOR PLASMA COLLAPSE IN EDGE2D-EIRENE AND SOLPS RUNS

As shown in the previous section, the smooth evolution of the SOL and divertor parameters ceases at a given n_u in both SOLPS4.3 and EDGE2D-EIRENE. If the gas puffing rate at this point increases further, the run evolves quickly towards a state where J_{sat} becomes close to zero (full detachment) and virtually all the recycling occurs inside the separatrix. We consider this transition in more detail here.

As discussed in Section 4.4 and [21], the roll-over and decrease of Jsat can be obtained by the reduction of the particle source in the divertor by an increase of the volume recombination source and/or a decrease of the ionization source. The latter effect could be due to the neutral-ion collisions which has the potential to slow down the recycling neutrals. Whether this process participates to the detachment or not, the neutral-ion collisions, involving atoms first (when the target T_e is above 1eV) and then molecules (when the target T_e is below 1eV), are important for the stability of the plasma. It is also worth noting that when the elastic molecule-ion collisions replace the charge-exchange, both processes occur with a similar rate [33].

It has been shown in Section 4.7 (Fig.19) that volume recombination - dominant at $T_e \sim 1$eV – is of the same order or stronger in experiment than in simulation. The plasma in the divertor must therefore be cold and dense, with a large fraction of neutrals downstream. As a consequence, the plasma pressure near the target must be low since $J_{sat} \propto pT^{-1/2}$. This means that a significant pressure gradient must be maintained in the divertor to match the high plasma pressure upstream in the SOL. According to the present work and other previous theoretical and modelling studies (see e.g., [15,38]), the neutrals play the key role in the formation of the pressure gradient and in dissipation of the power in the divertor. However, the abundance of neutrals is detrimental for the core plasma performance, so the neutrals must be contained in the divertor, plugged by the plasma.

The sharp evolution of the code runs with increasing upstream density suggests some kind of a bifurcation where a stable branch of the solution disappears at a given density. It was shown in [39] that a rapid increase of the neutral outflow from the divertor once the total particle content in the edge exceeds some critical level should be the most prominent feature of such a bifurcation. This allows one to build a qualitative picture of the plasma collapse in the SOLPS4.3 and EDGE2D-EIRENE runs. The evolution of some plasma parameters during the collapse is shown in Fig.26. These calculations were performed with SOLPS4.3 starting from the last stable point in the density ramp and increasing the gas puffing rate by 2%.

Initially the run develops smoothly. The particle content outside the separatrix increases slowly, J_{sat} decreases and neutral-related radiation from the core increases. Then at ~2.7ms a bifurcation occurs. The neutrals start leaving the divertor and reaching the core. The radiation from the core grows, the SOL power (PSOL) decreases accordingly and leads to the reduction of Jsat. At ~3.8ms the radiation from the core (mostly C) exceeds the input power, cooling the plasma, PSOL 0 and Jsat decreases further. As a result, the pumping becomes less efficient but the gas puff continues and the particle content in the edge increases. The neutrals fill the SOL and reach the targets, thus the pumping recovers, and at ~4.5ms the run nearly reaches a new steady state, where most of the

recycling occurs in the core and the edge is dominated by neutrals. In these runs, the boundary conditions at the innermost closed flux surface (the core boundary) were set to ensure constant power flux from the core and an ion outflux balancing the neutral influx across this surface. In reality, such a massive penetration of neutrals to the core should cool the whole core and likely lead to a disruption.

In this picture, the effect of the elastic molecule-ion collisions (Section 5) can be attributed to their contribution to the neutral confinement in the divertor, when the charge-exchange does not occur anymore because of the lack of recycling atoms. Indeed, without these processes in the model, the molecules produced by the recycling, when the target T_e is below 1eV, penetrate the cold plasma of any density freely, without interaction. The elastic molecule-ion collisions make this transport diffusive thus creating a gradient in the molecule density. When the target T_e is above 1eV, the charge-exchange does the same with the recycling atoms.

Apparently, the stabilizing effect of the radiation trapping in the dense neutral gas [40] is similar in nature. Having absorbed a Lyman series photon, the neutral excites and can be efficiently ionized at low T_e, and this reduces its probability to reach the hot core.

8. IN-OUT DIVERTOR ASYMMETRY IN SIMULATIONS AND EXPERIMENTS

The experimentally observed in-out asymmetric detachment is not reproduced by EDGE2D-EIRENE in the cases presented here. Two attempts have been made to artificially introduce a power asymmetry with a model in which the power is distributed preferentially on the outer divertor: $P_{OT} \approx 2P_{IT}$ and $P_{OT} \approx 3P_{IT}$. To do so, the inner and outer divertors must be simulated by separate runs, but the total amount of power entering the divertor is the same as in the reference simulation (~3MW). The results from these EDGE2D-EIRENE simulations are compared with the J_{sat} and T_e measurements (see Figs.27 and 28) from LP #02 and #18 on JET-C and the LP #02 and #15 (see Fig.25) on JET-ILW. The error bars on the simulation results show the consequence of an uncertainty of plus or minus one cell on the position of the LP on the grid. The error can be important since J_{sat} and T_e gradients can be significant on the target profiles around the strike point (see Figs.7 and 9).

If a phenomenon capable of generating a deficit of power between the inner and outer SOL exists, it would have as a consequence an earlier detachment on the IT as shown by the evolution of J_{sat} in Fig.27 for the both simulated impurities, C and Be. Earlier detachment in experiment compared with simulation may in this case be a consequence of E×B drifts and parallel currents as suggested by [4,41] and [42] but no modelling attempt including these effects is made here.

To reach the maximum experimental value of J_{sat} at a given location on the IT and the OT, the IT needs to receive 2 to 3 times less power than the OT (see Fig.27). However, even if the experimental trend is qualitatively reproduced by this model, the mismatch in the value of n_u at which detachment occurs, even accounting for the uncertainty on the separatrix position, remains significant. The inclusion of approximate corrections on the experimental probe data due to the polarization drift on the OT (see Section 4.2) allows the evolution of the measured T_e to approach

more closely the simulations for the cases $P_{OT} \approx 2P_{IT}$ and $P_{OT} \approx 3P_{IT.}$ Figure 27 clearly shows that for both the JET-C and JET-ILW density ramps, the particle flux rollover is always followed by a fast decrease of J_{sat}, while the latter stagnates in the simulations and shows a similar behaviour as observed experimentally only at the last simulated upstream density point of the ramp.

CONCLUSIONS

Results from EDGE2D-EIRENE simulations of JET L-mode, low power density ramps with high triangularity configuration with either C or Be impurities have been compared to well matched (with the exception of working gas), reasonably well diagnosed JET-C and JET-ILW experiments.

This detachment modelling appears to be strongly sensitive to the atomic physics. The simulations reproduce reasonably well the experimental conditions for the low recycling, high recycling, partially detached and strongly detached regimes at the OT in JET-C and JET-ILW only if elastic collisions between ions and molecules are included in the EIRENE neutral model, as in [2,3]. The code can better match the experimental in-out power asymmetry if the heat flux entering the outer divertor is artificially set at around 2–3 times the heat flux entering the inner divertor. A further outcome of this work has been to demonstrate that key JET divertor diagnostic signals – T_e from LP and bolometric tomographic reconstructions - are running in the limit of validity in high recycling and detached conditions and cannot be reliably used for code validation. The simulations do, however, reproduce rather well the evolution of the line integrated bolometer chord measurements.

The detachment appears to be essentially similar in both environments in simulations and experiments, except for the upstream density limit found 20% to 30% higher JET-ILW than with the JET-C (as in [17]). Amongst many possible effects responsible for the overestimation of T_e measured by the LP at high density in the divertor, the influence of the polarization drift has been estimated here with [20]. Once this effect is subtracted, the OT T_e measurements from the JET experiments studied here can drop significantly (factor 2–4), confirming the strong and fast decrease of T_e obtained by the simulations and suggested by the IR measurements. The inclusion of this correction would bring significant portions of the JET-C and JET-ILW experimental target T_e profiles around 1eV and below for the partially detached and strongly detached phases.

In both environments, these experimental conditions would be compatible with the presence of a strong volume recombination source during the detachment process which is confirmed by the spectroscopy of high-n H or D line radiation and the EDGE2D-EIRENE simulations, consistently with [21]. Comparison between simulation results and two-point modelling suggests that the volume recombination seems to have a stronger effect on the IT than on the OT detachment. However, it is not yet clear if the experimental detachment is produced by the observed increase of volume recombination and/or a possible - but not experimentally verified - decrease of the ionization source due to neutral-ion collisions.

In JET-C, the simulated distribution of the radiative power is remarkably similar to the bolometric chord measurements. In the simulations with Be impurities, the strong assumption that the W divertor

is entirely coated with Be appears to be exaggerated but the overestimated contribution of the latter to the divertor radiative power is not sufficient to retrieve the experimental measurements for the same region. One or several other sources of radiation seem to be involved in the JET-ILW experiment (remaining radiative impurities, stronger contribution from D and/or stronger contribution from the core). However, the general pattern of the experimental radiative power distribution showing a maximum around the X-point, as in JET-C, is reproduced by the code for the JET-ILW experiment. The good match obtained for the bolometric LOS in the JET-C discharge is not found with the tomography, casting severe doubt on the uniqueness of the reconstruction.

It is worth mentioning that the target T_e threshold, set at 1eV in EIRENE to allow the recycling to switch from atomic to molecular, is a key parameter to trigger the massive production of molecules required for the elastic molecule-ion collisions to become significant. However, this value, set identical for any wall material (C or Be here) in EIRENE, is somewhat arbitrary since in reality, the switch from atomic to molecular recycling is possibly a smooth process starting at higher temperature than 1eV and strongly material dependent [34,35]. Since the rate of the elastic molecule-ion collisions does not change much with T_e [33] a higher threshold may have an impact on the modelling of the detachment.

Comparison between EDGE2D-EIRENE and SOLPS4.3 simulations of the JET-C density ramp, with both codes employing identical versions of the EIRENE Monte-Carlo neutral package, shows that the detachment trends are similar. This gives some comfort that the simulation predictions from SOLPS4.3 for ITER divertor operations are reasonable. In both codes, molecule-ion collisions appear to improve neutral confinement in the divertor at low temperature, when the molecular recycling dominates over the atomic recycling. If the elastic molecule-ion collisions are not included in SOLPS4.3 and EDGE2D-EIRENE simulations, the molecules massively penetrate the core plasma and lead to a bifurcated state where the bulk of the ionization source is into the core. In this case, the bifurcated solution occurs before the appearance of a stable strongly detached solution and provides a plausible explanation as to why the detachment signature is not clearly obtained in the simulations involving the NIMBUS-like set of atomic physics reactions.

ACKNOWLEDGEMENTS

This work was supported by EURATOM and carried out within the framework of the European Fusion Development Agreement. The views and opinions expressed herein do not necessarily reflect those of the European Commission.

REFERENCES

[1]. R.A. Pitts et al., Journal of Nuclear Materials **415** (2011) S957–S964
[2]. V. Kotov et al., Plasma Physics and Controlled Fusion **50** (2008) 105012
[3]. M. Wischmeier et al., Journal of Nuclear Materials **523–529** (2011) 415
[4]. M. Groth et al., Journal of Nuclear Materials **415** (2011) S530–S534

[5]. R. Simonini et al., Contribution to Plasma Physics **34** (1994) 368
[6]. S. Wiesen, www.eirene.de/e2deir_report_30jun06.pdf
[7]. A.S. Kukushkin et al., Nuclear Fusion **49** (2009) 075008
[8]. C.F. Maggi et al 1999 Nuclear Fusion **39** 979
[9]. E. Tsitrone et al., Plasma Phys. Control. Fusion **44** (2002) 701–71
[10]. V. Philipps et al., Journal of Nuclear Materials **438** (2013) S1067–S1071]).
[11]. W. Fundamenski, Plasma Phys. Control. Fusion **47** (2005) R163-R208].
[12]. J.W. Davis et al., Journal of Nuclear Materials **241–243** (1997) 37
[13]. K. Krieger et al. Journal of Nuclear Materials **438** (2013) S262–S266
[14]. C. Guillemaut et al., Journal of Nuclear Materials **438** (2013) S638–S642
[15]. P.C. Stangeby, The plasma boundary of magnetic fusion devices, IOP publishing (2000)
[16]. A. Kallenbach et al., Journal of Nuclear Materials **337–339** (2005) 381–385
[17]. M. Groth et al., Journal of Nuclear Materials **438** (2013) S175–S179
[18]. R. Dejarnac et al., Plasma Physics and Controlled Fusion **49** (2007) 1791–1808
[19]. J.P. Gunn et al., Review of Scientific Instruments **66**, 154 (1995)
[20]. A. Carlson and M. Weinlich, Contribution to Plasma Physics **38** (1998) S, 38-46
[21]. S.I. Krasheninnikov et al., Physics ofPlasmas **4** (5), 1638-1646, May 1997
[22]. S. Marsen et al., Journal of Nuclear Materials **438** (2013) S393-S396
[23]. C.S. Pitcher & P.C.Stangeby, Plasma Physics and Controlled Fusion **39** (1997) 779–930
[24]. S.A. Self and H.N.Ewald, Physics of Fluids **9**, 2486 (1966)
[25]. R.K. Janev et al., Elementary processes in H and He plasmas, Springer, 1987
[26]. G.F. Matthews et al., Journal of Nuclear Materials **438** (2013) S2–S10
[27]. M. Groth et al., Nuclear Fusion **53** (2013) 093016
[28]. S.Brezinsek, Journal of Nuclear Materials **438** (2013) S303–S308
[29]. http://www.adas.ac.uk
[30]. A. Widdowson et al., PFMC Conference, Jülich, 2013
[31]. A.G. Meigs et al., Journal of Nuclear Materials **438** (213) S607-S611
[32]. V. Kotov and D. Reiter, Plasma Physics and Controlled Fusion **51** (2009) 115002
[33]. http://www.eirene.de/manuals/amjuel.pdf
[34]. S. Brezinsek et al., Journal of Nuclear Materials **313–316** (2003) 967–971
[35]. S. Markelj et al., The Journal of Chemical Physics, **134**, 124707 (2011)
[36]. A.S. Kukushkin et al., Fusion Engineering and Design **86** (2011) 2865
[37]. V. Kotov et al., Contribution to Plasma Physics **50**, No. 3-5 (2010)
[38]. A.S. Kukushkin et al., Journal of Nuclear Materials **438** (2013) S203
[39]. S.I. Krasheninnikov et al., Journal of Nuclear Materials. **266-269** (1999) 251-257
[40]. V. Kotov, Journal of Nuclear Materials **438** (2013) S449–S452
[41]. V. Rozhansky et al., Journal of Nuclear Materials **438** (2013) S297–S302
[42]. L. Aho-Mantila et al., Journal of Nuclear Materials **438** (2013) S321–S325

Experiment (C)	n_u (m^{-3})	1.1 x 10^{19}	1.3 x 10^{19}	1.7 x 10^{19}	2.1 x 10^{19}
	P_{heat} (MW)	2.7	2.7	2.9	3.2
	P_{rad} (MW)	0.5	0.9	1.3	1.9
	P_{IT} (MW)	~ 0.6	~ 0.5	~ 0.01	~ 0.01
	P_{OT} (MW)	< 1.1	< 0.9	< 0.8	< 0.7
	P_{loss} (MW)	> 0.5	> 0.4	> 0.7	> 0.5
	P_{loss} (%)	> 19 %	> 15 %	> 28 %	> 19 %
Code	P_{heat} (MW)	3	3	3	3
	P_{loss} (MW)	0.6	0.76	0.77	0.55
	P_{loss} (%)	20 %	25 %	26 %	18 %

Table 1: Power balance in C experiment and simulation.

C	n_u (10^{19} m^{-3})	1.1	1.3	1.5	1.7	2
	Albedo	0.84	0.90	0.94	0.97	0.98
Be	n_u (10^{19} m^{-3})	1.2	1.5	1.7	2.1	2.6
	Albedo	0.86	0.90	0.93	0.96	0.97

Table 2: Evolution of vessel wall Albedo for the simulation with C and Be impurities.

NIMBUS-like model	**Kotov-2008 model**
(1) $e + H^0 \rightarrow 2e + H^+$	Same reactions as default plus:
(2) $H^+ + H^0 \rightarrow H^0 + H^+$	(9) $H_2 + H^+ \rightarrow H^+ + H_2$
(3) $e + C^0 \rightarrow 2e + C^+$	(10) $H_2 + H^+ \rightarrow H_2^+ + H^0$
(4) $e + H_2 \rightarrow 3e + 2H^+$	(11) $e + H_2 \rightarrow 2e- + H_2^+$
(5) $e + H_2 \rightarrow e + 2H^0$	(replacing (4))
(6) $e + H_2 \rightarrow 2e + H^+ + H^0$	(12) $e + H_2^+ \rightarrow e + H^0 + H^+$
(7) $e + H^+ \rightarrow H^0$	(13) $e + H_2^+ \rightarrow 2e + 2H^+$
(8) $2e + H^+ \rightarrow e + H^0$	(14) $e + H_2^+ \rightarrow 2H^0$
No CRM for (4), (5) and (6)	CRM for (11), (5) and (6)

Table 3: Atomic and molecular reactions included in the physics models used in EIRENE.

Quantity	**Value**	**Comment**
R	3 m	Major Radius
a	1 m	Minor radius
q_{95}	5	Safety Factor
λ_q	1 cm	Power decay length
I_p	2x10^6 A	Plasma current
B_t	3.1 T	Toroidal field
P_{heat}	3x10^6 W	Heating power
P_{rad_core}	0.5x10^6 W	Core radiative power
$L_{//}$	≈ 50 m	Average connection length
γ	7	Sheath transmission coefficient
m_i	1.67x10^{-27} kg	Main ion mass
L_z	2x10^{-32} W.m^{-3}	Radiative Power Coefficient at 3 eV
c_z	2 %	Radiating impurity concentration
L_{rec}	10 m	Recombination length

Table 4: Parameters used in the two-point model here.

	Environment	JET- C (Pulse No: 79315)	JET- ILW (Pulse No: 82342)
Exp.	Core P_{rad} (MW)	0.2 (8 %) → 0.5 (16 %)	0.6 (18 %) → 0.7 (19 %)
	Divertor P_{rad} (MW)	0.4 (15 %) → 1.6 (50%)	0.9 (26 %) → 1.5 (40%)
	Total P_{rad} (MW)	0.6 (23 %) → 2.1 (66%)	1.5 (44 %) → 2.2 (59%)
Code	H or D P_{rad} (MW)	0.14 (5 %) → 0.44 (15 %)	0.21 (7 %) → 0.44 (15 %)
	Impurity P_{rad} (MW)	0.44 (14 %) → 1.05 (35 %)	0.19 (6 %) → 0.44 (15 %)
	Total P_{rad} (MW)	0.58 (19 %) → 1.49 (50 %)	0.4 (13 %) → 0.88 (29 %)

Table 5: Evolution of the radiated power and fraction of the input power radiated in the code and experiment.

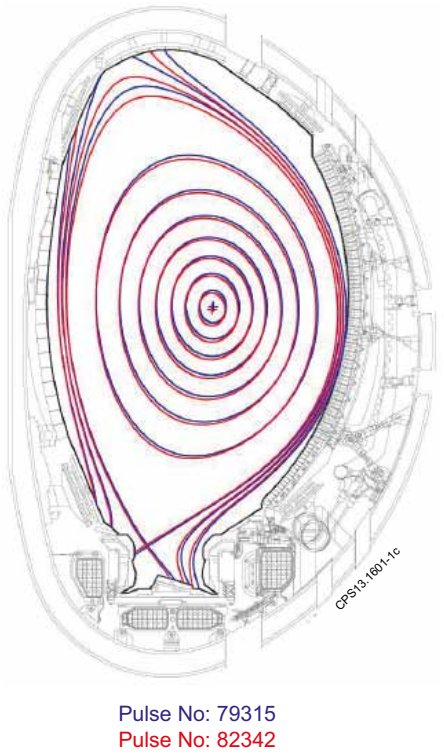

Figure 1: Magnetic equilibria for the Pulse No's: 79315 and 82342 at 20s and 13s respectively.

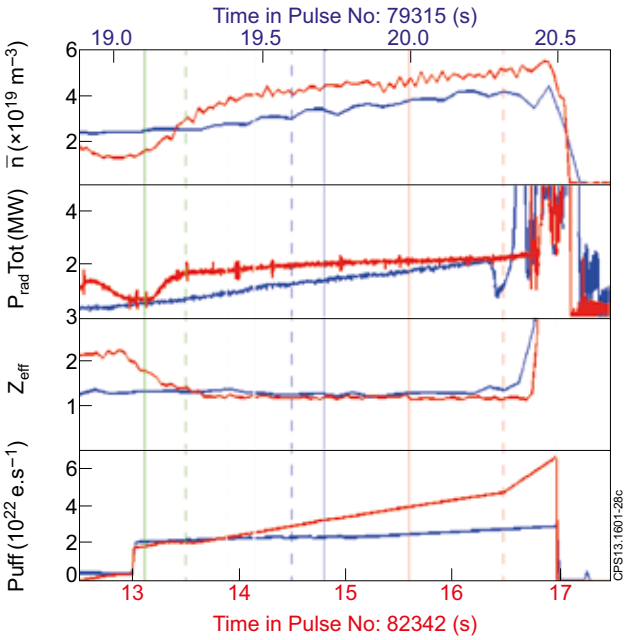

Figure 2: Time traces for the JET-C and JET-ILW discharges (blue and red respectively). From top to bottom: line averaged density, total radiative power, Z_{eff} and gas injection flux. The vertical lines represent the time slices in JET-C (plain lines) and JET-ILW (dashed lines) for the low recycling (green), high recycling (black), partially detached (blue) and strongly detached (red) conditions.

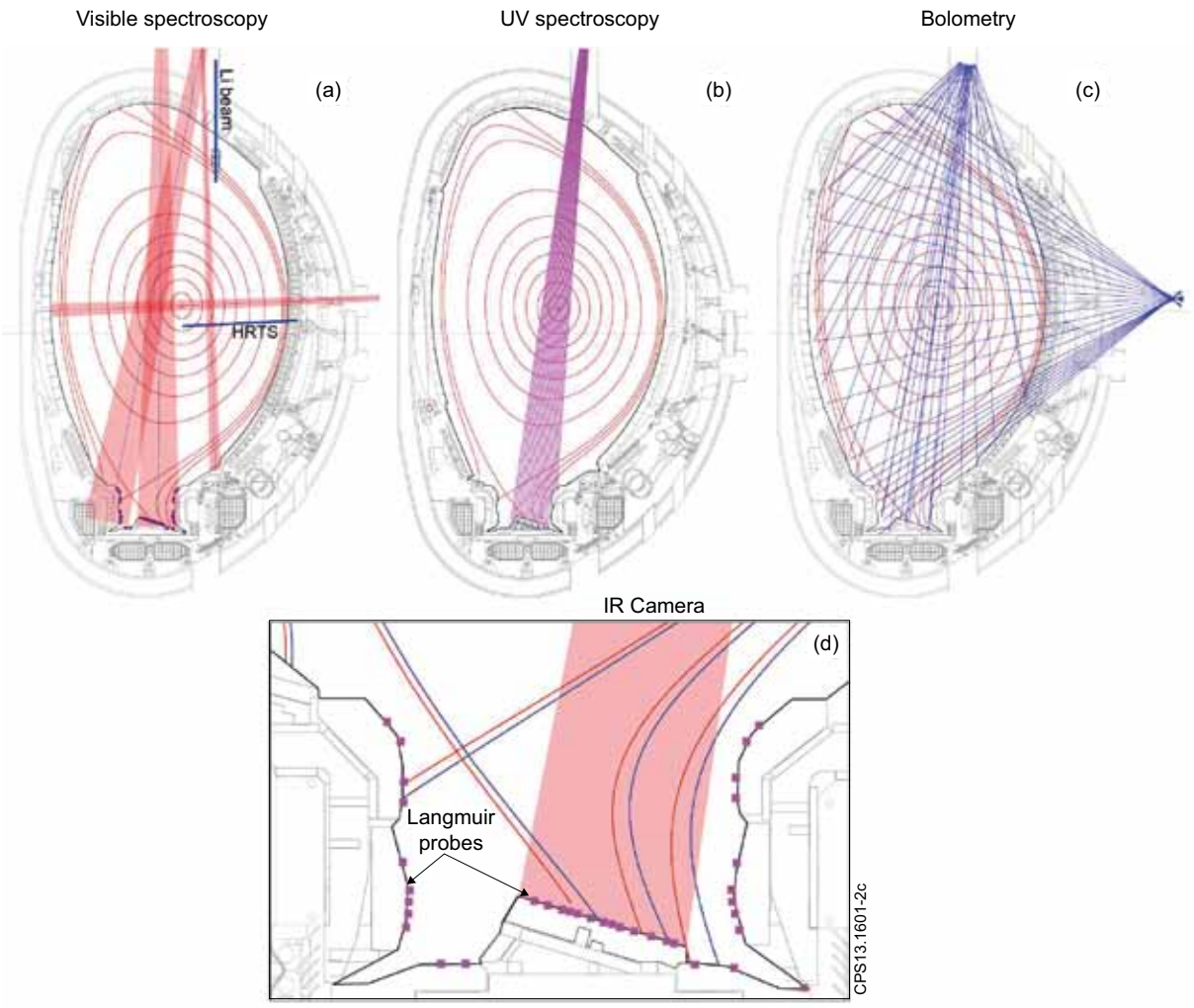

Figure 3: a) Visible spectroscopy lines of sight (LOS), Lithium beam (Li-beam), HRTS and divertor LP, b) UV spectroscopy LOS, c) bolometer LOS, d) zoom of the divertor with Langmuir probes (LP) and IR camera field of view (FOV).

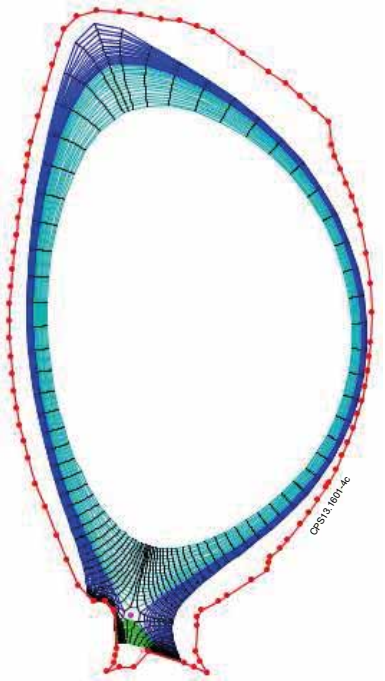

Figure 4: Modified EDGE2D grid

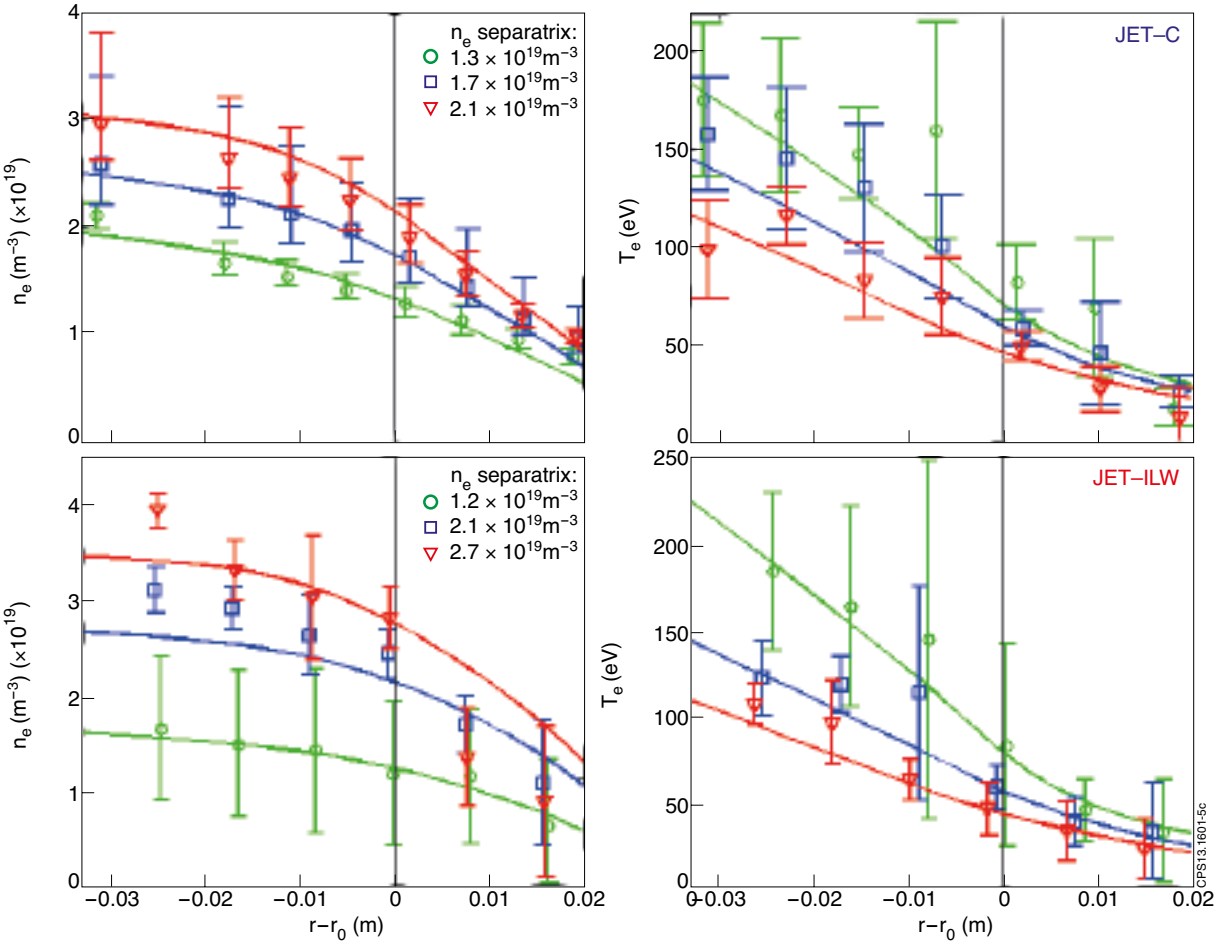

Figure 5: Upper row from left to right: EDGE2D-EIRENE model (curves) and experimentally measured (points with error bars) n_u and T_u profiles (Li-beam and HRTS respectively) at 3 different points in the density ramp for the JET-C discharge. Lower row from left to right: as above but for the JET-ILW discharge (HRTS only). Only 3 profiles are shown for clarity.

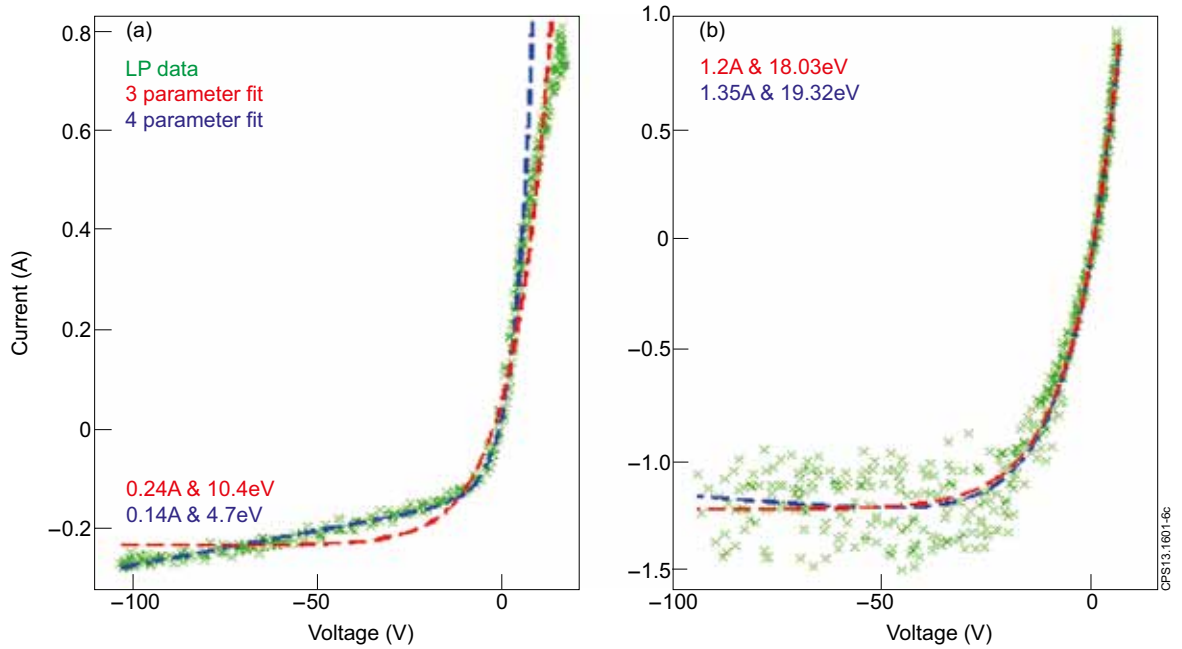

Figure 6: a) Examples of experimental current-voltage characteristics with 3 and 4–parameter fits obtained at low T_e in the C experiment, b) the same but at high T_e.

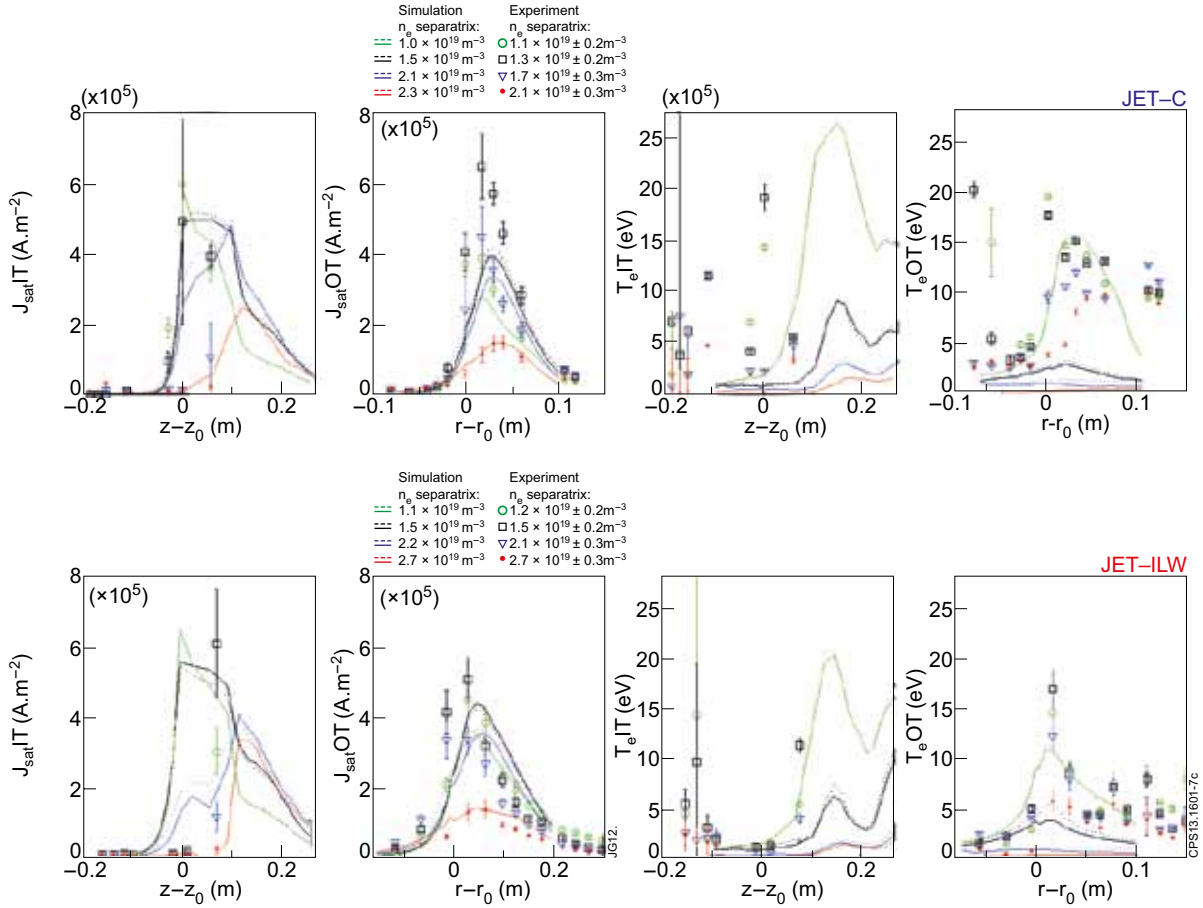

Figure 7: Comparison between EDGE2D-EIRENE simulations (solid lines for Kotov-2008 neutral model and dashed for NIMBUS-like neutral model) and experimental LP data (error bars) during the density ramps in JET-C (upper) and JET-ILW (lower). From left to right: IT and OT J_{sat}, IT and OT T_e.

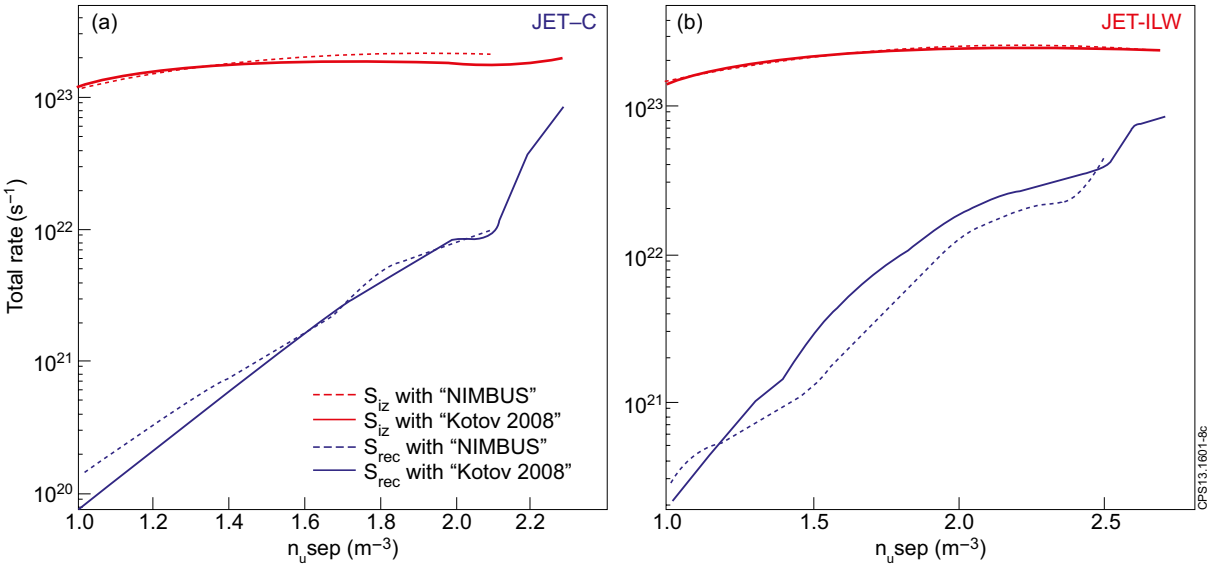

Figure 8: a) Evolution of the total ionization and volume recombination rate in EDGE2DEIRENE simulations with C impurities, b) the same but with Be impurities.

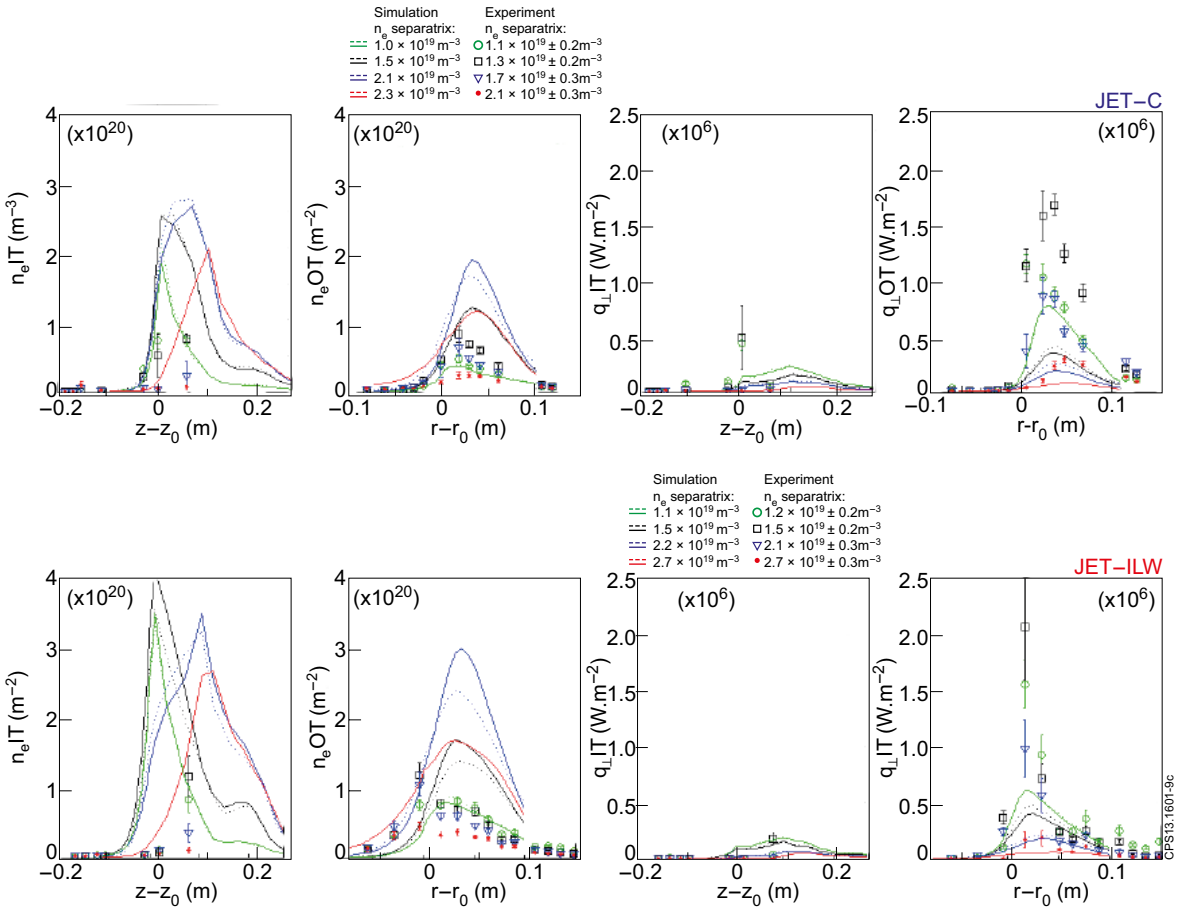

Figure 9: Comparison between EDGE2D-EIRENE simulations (solid lines for Kotov-2008 neutral model and dashed for NIMBUS-like neutral model) and experimental LP data (error bars) during the density ramps in JET-C (upper) and JET-ILW (lower). From left to right: IT and OT electron density, IT and OT parallel heat flux density.

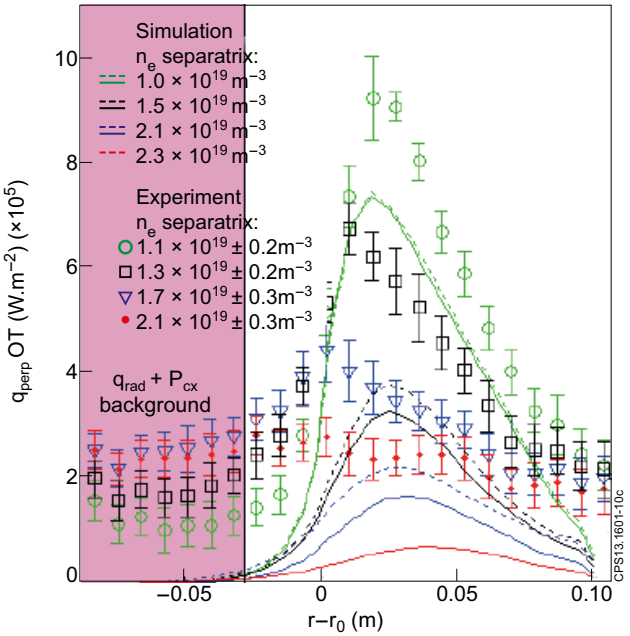

Figure 10: Comparison between EDGE2D-EIRENE simulations and IR data for the density ramp with C PFC (solid lines for Kotov-2008 neutral model and dashed for NIMBUS-like neutral model). Shaded domain corresponds to the PFR averaging region.

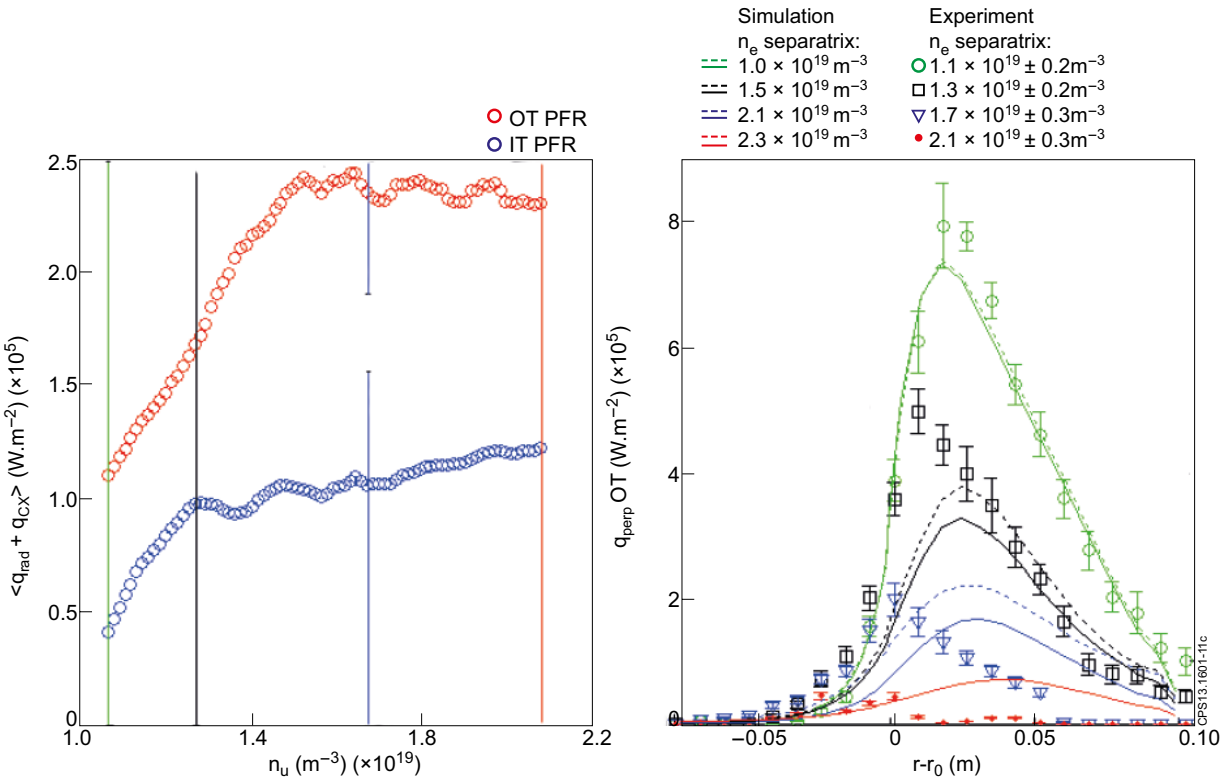

Figure 11: a) Average experimental heat flux density in the inner and outer PFR, b) simulation curves from Fig.10 with the reprocessed IR OT power deposition profile obtained by subtraction of the PFR heat flux at each of the four selected times.

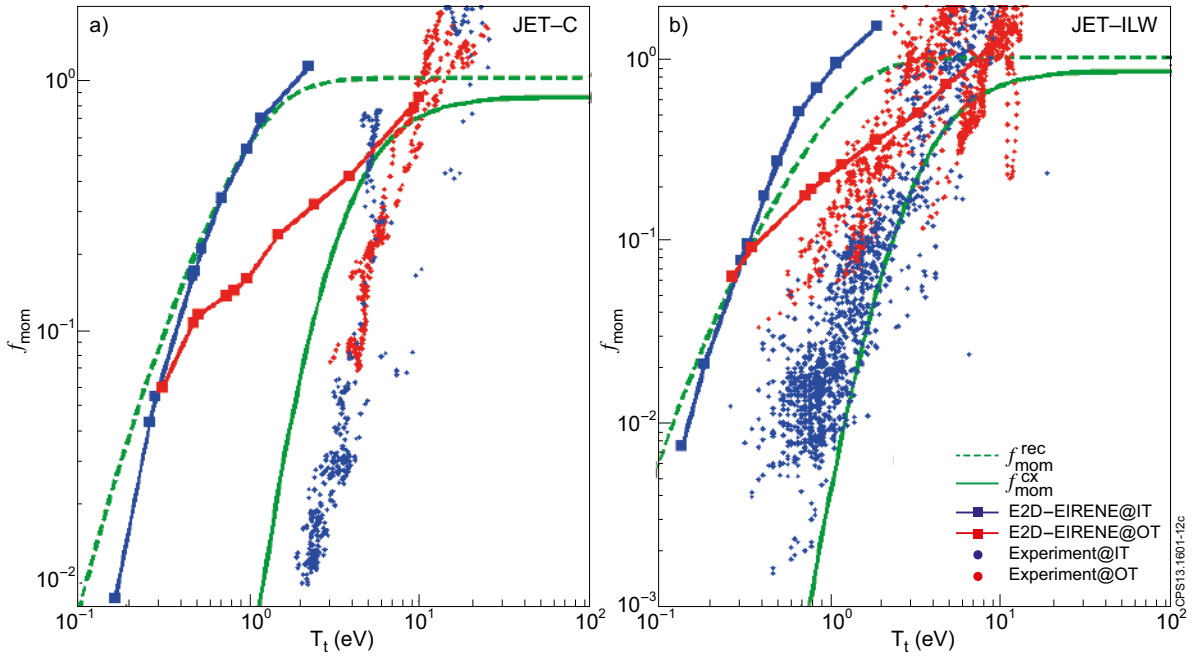

Figure 12: Downstream to upstream pressure ratios given by the Self and Ewald formula, the experiment and the EDGE2D-EIRENE simulations for C impurities (left) and Be impurities (right).

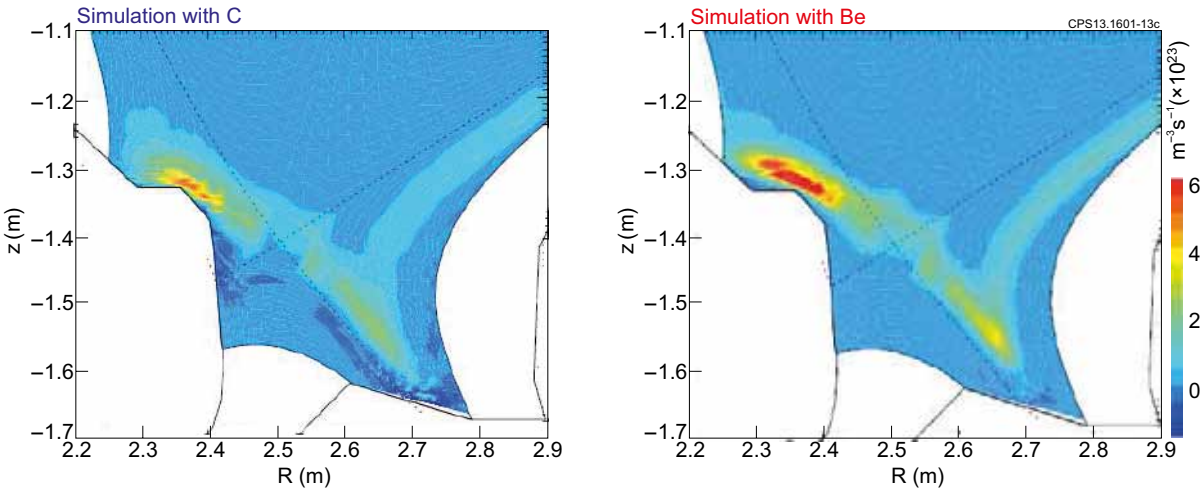

Figure 13: Ionization sources at the 3rd simulated point of the density ramps with C impurities (left) and Be impurities (right).

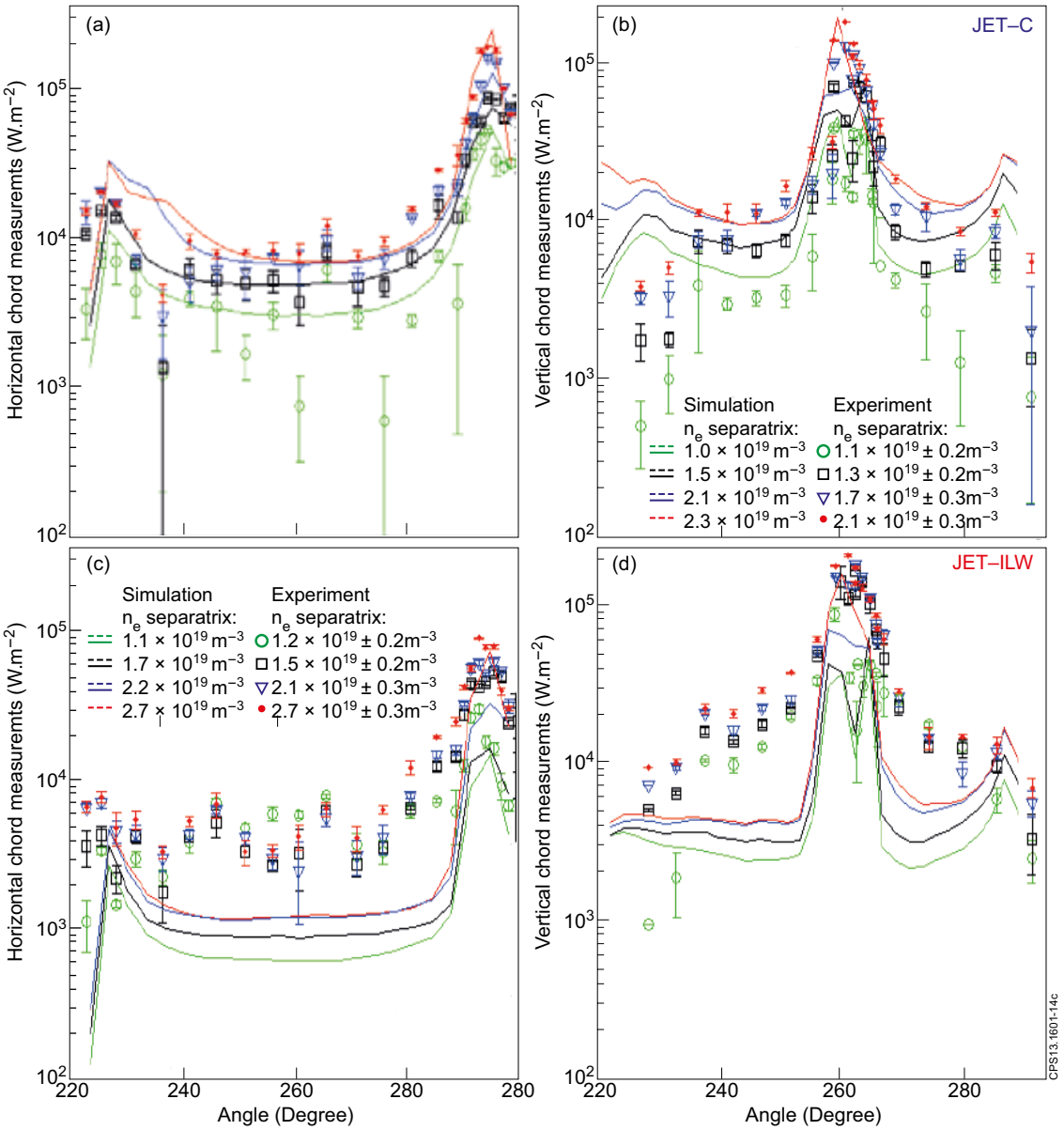

Figure 14: a) and b) code-experiment comparison of horizontal and vertical bolometer chord data for JET-C. c) and d) the same in JET-ILW.

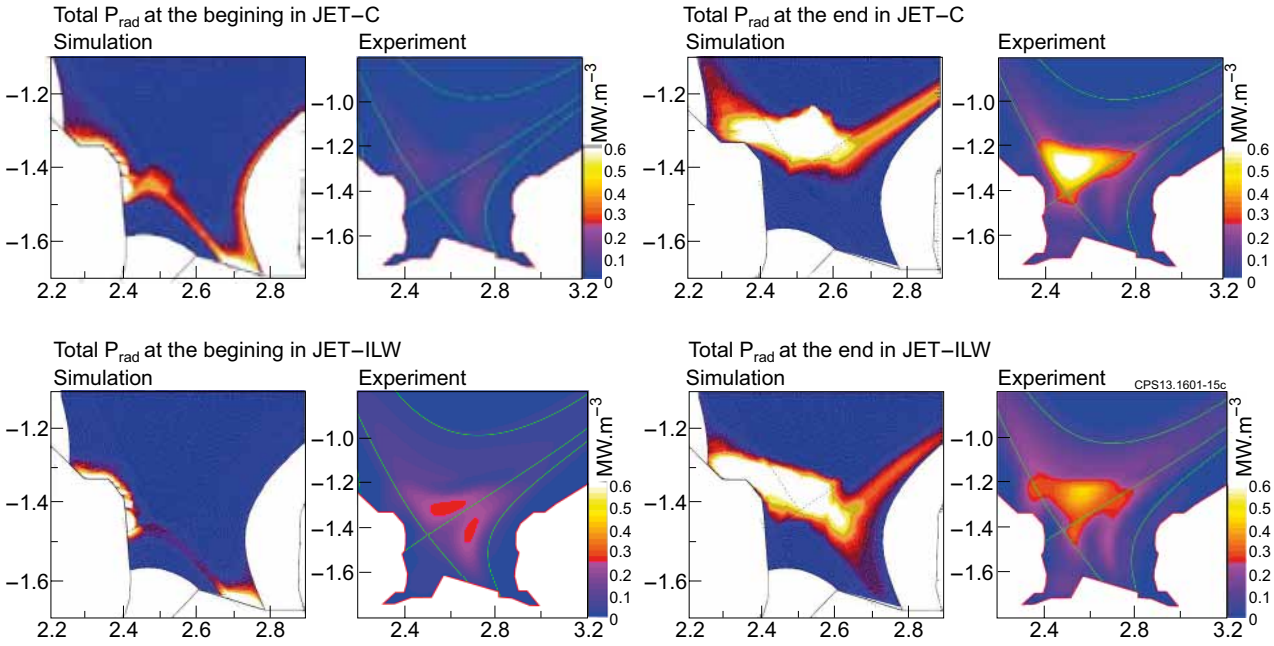

Figure 15: Comparison between EDGE2D-EIRENE simulations and tomographic reconstructions performed with the bolometric signals at the beginning and the end of both JET-C and JET-ILW density ramps.

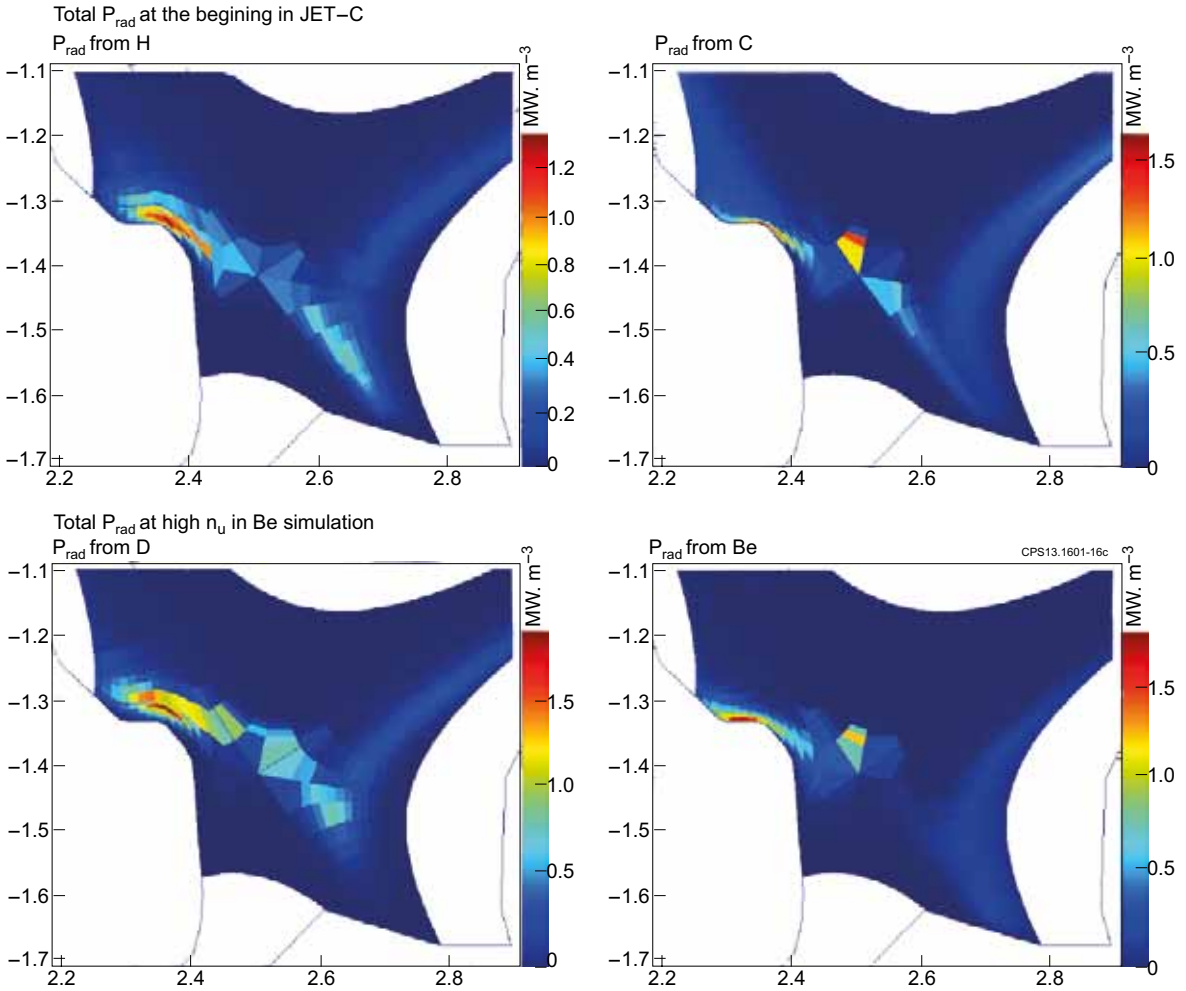

Figure 16: Top: distribution of H and C radiation in the EDGE2D-EIRENE simulations. Bottom: distributions of D and Be.

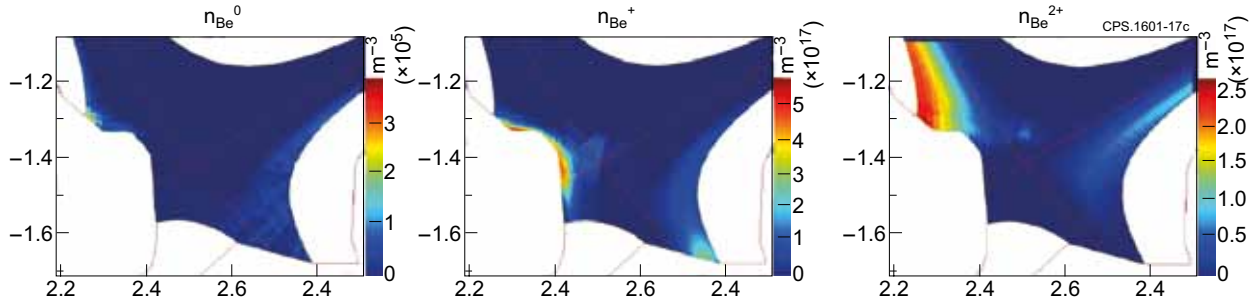

Figure 17: Density distributions of the main divertor impurity species in the EDGE2DEIRENE simulations with Be corresponding to the radiative power distribution in Fig.16.

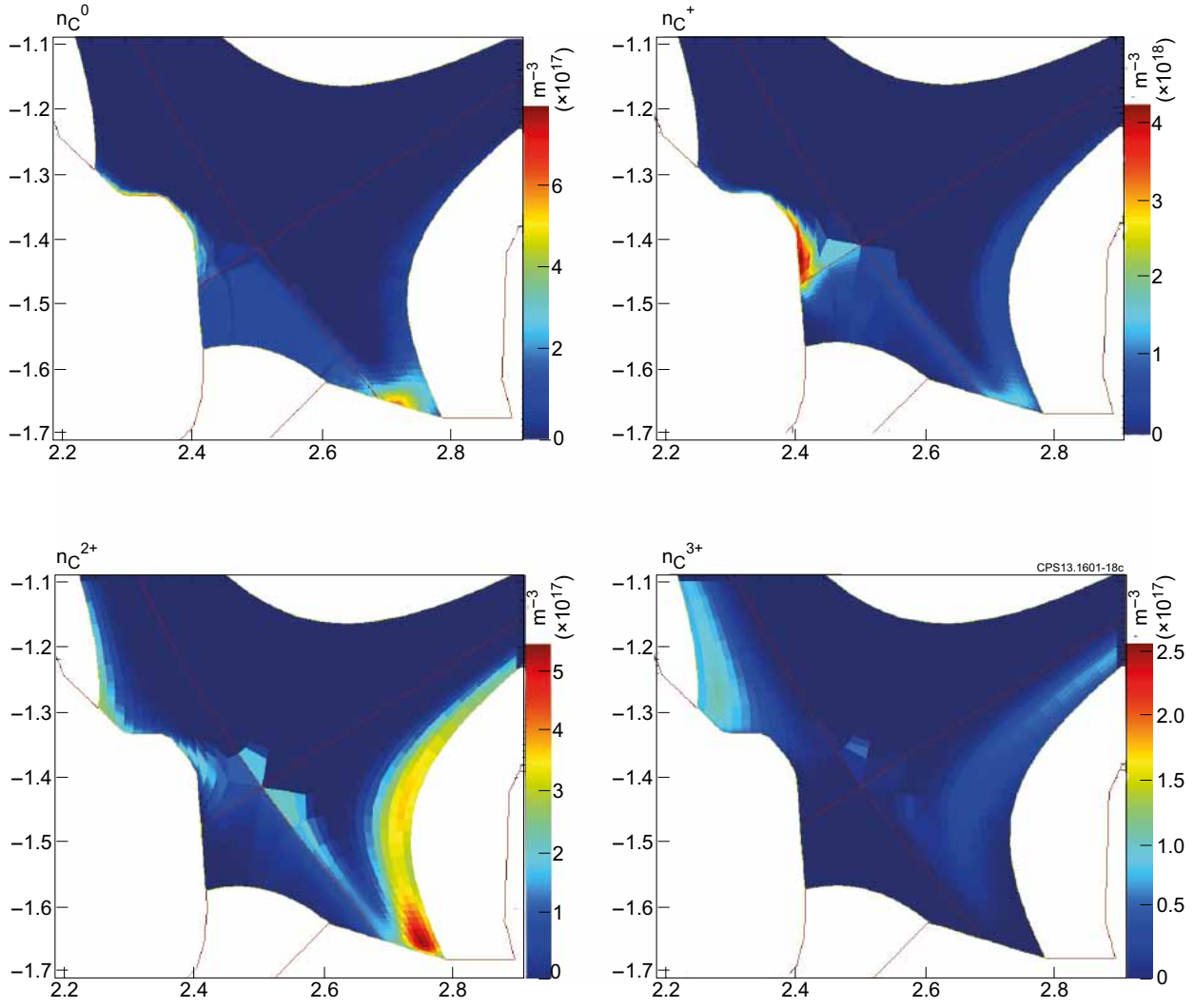

Figure 18: The same as Fig. 17 for the EDGE2D-EIRENE simulations with C.

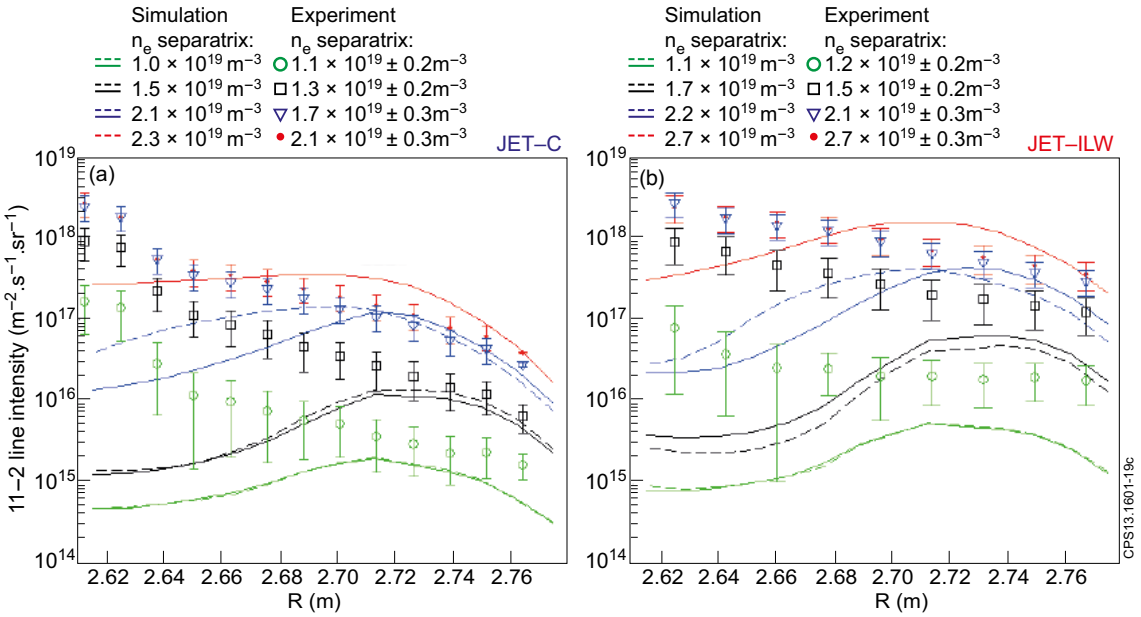

Figure 19: Code-experiment comparison of the evolution of 11-2 line intensity in JET-C, b) the same in JET-ILW.

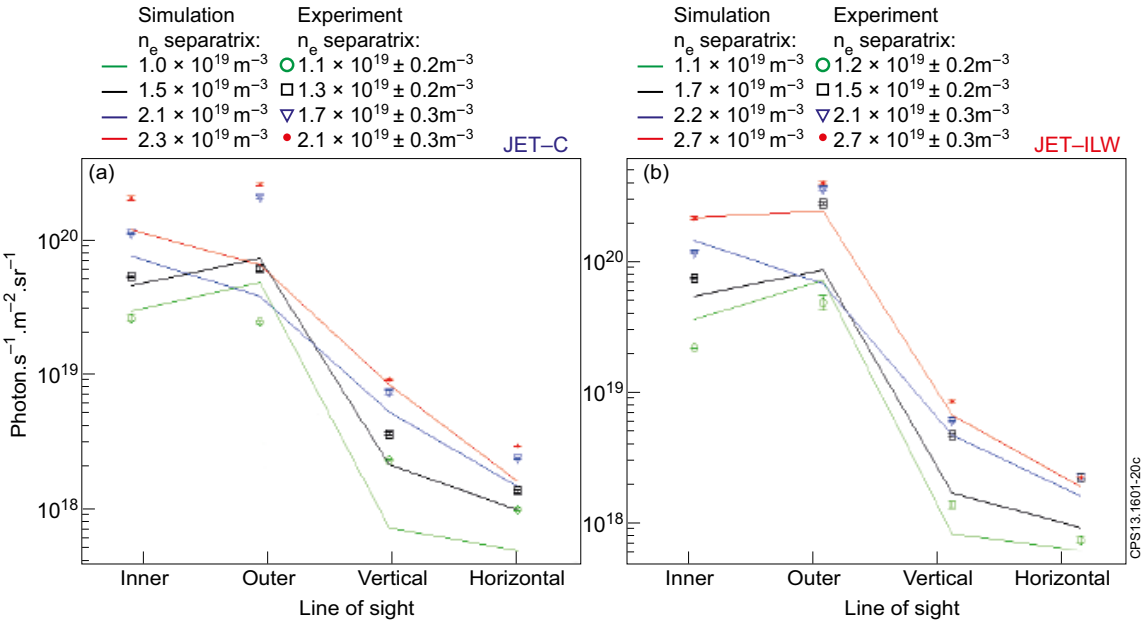

Figure 20: a) Comparison of experimental and simulated Hα line radiation intensities for the four LOS in the JET-C density ramp at the four standard density points, b) the same for the intensity of Dα lines in JET-ILW.

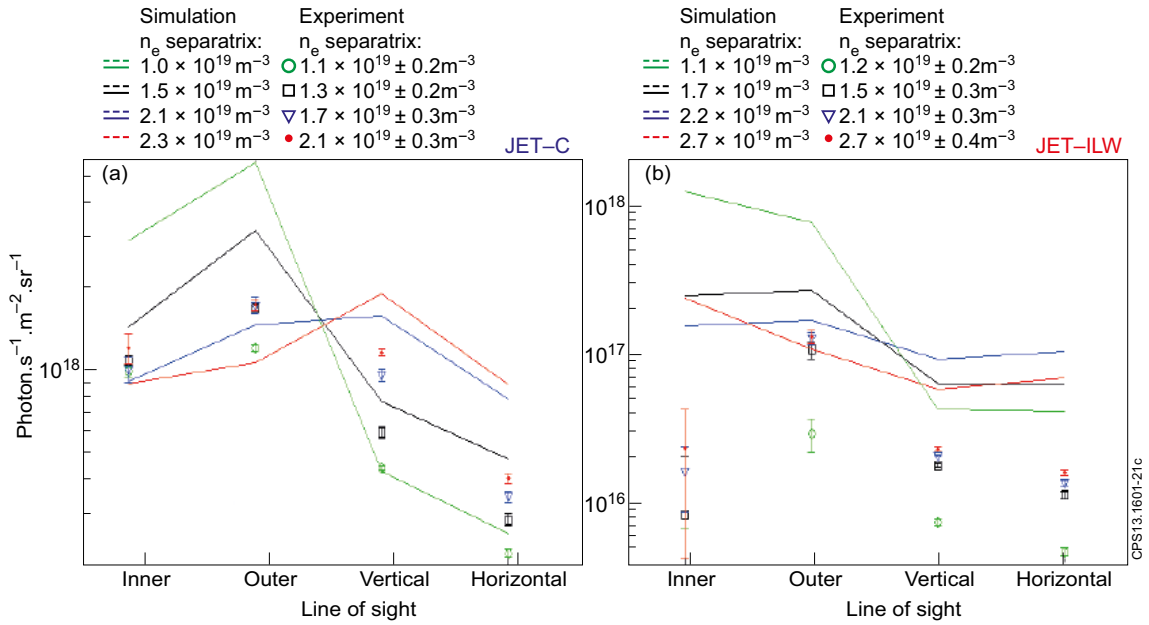

Figure 21: a) Code-experiment comparison of the evolution of the intensity of C^{2+}, b) the same for the intensity of Be+ lines.

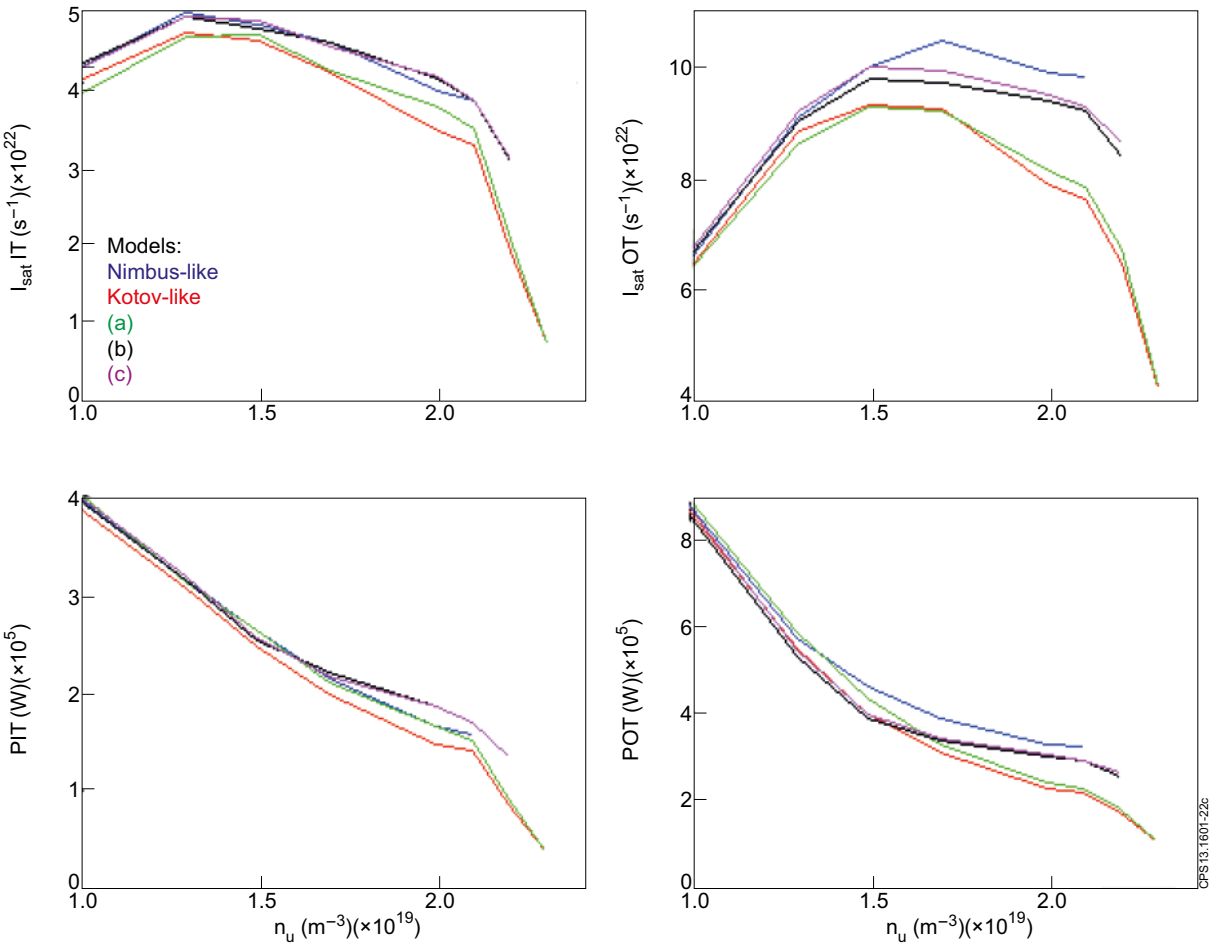

Figure 22: From left to right and top to bottom: integrated IT saturation current, integrated OT saturation current, integrated IT power deposition and integrated OT power deposition for 5 different AMD sets in EIRENE (see text).

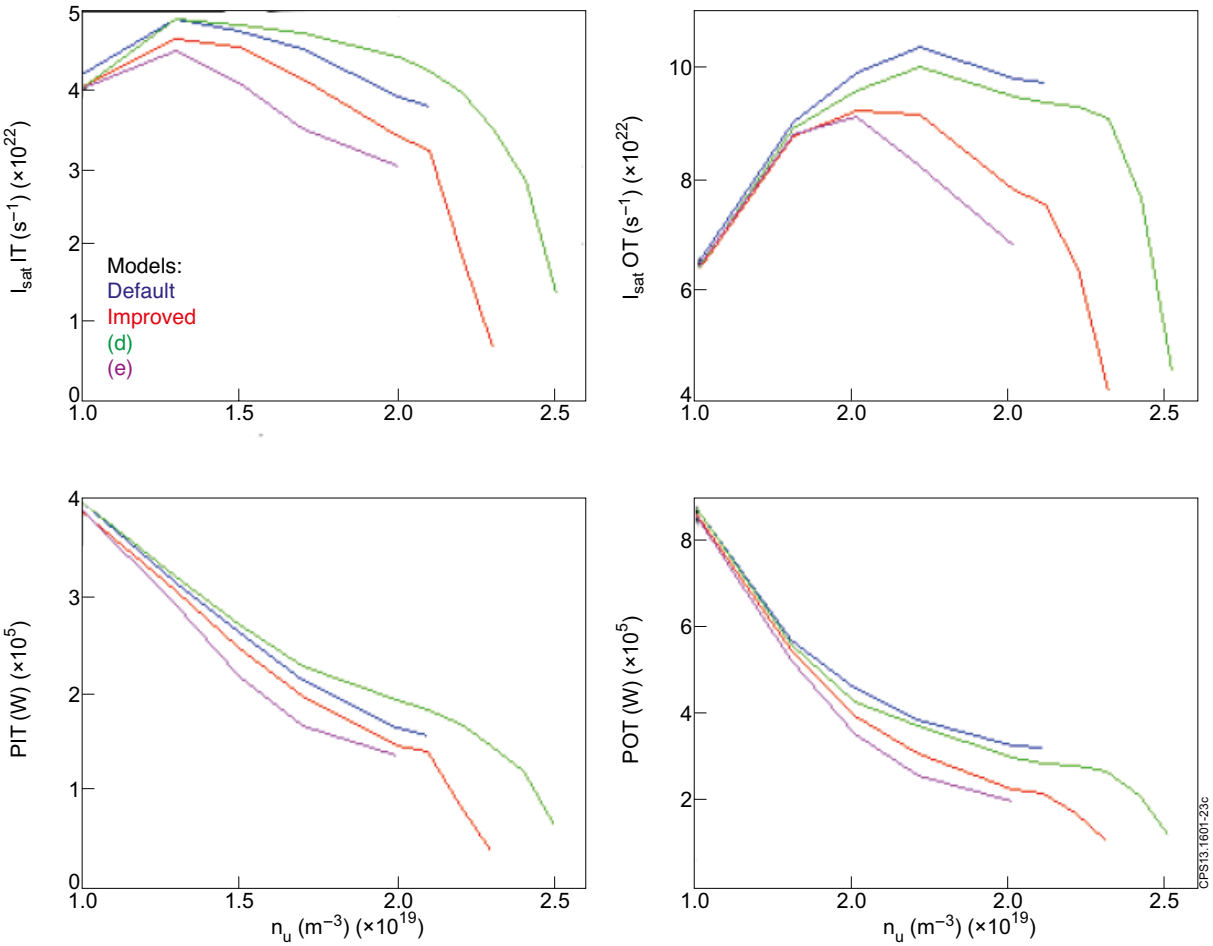

Figure 23: Same as Fig.22 for other AMD sets.

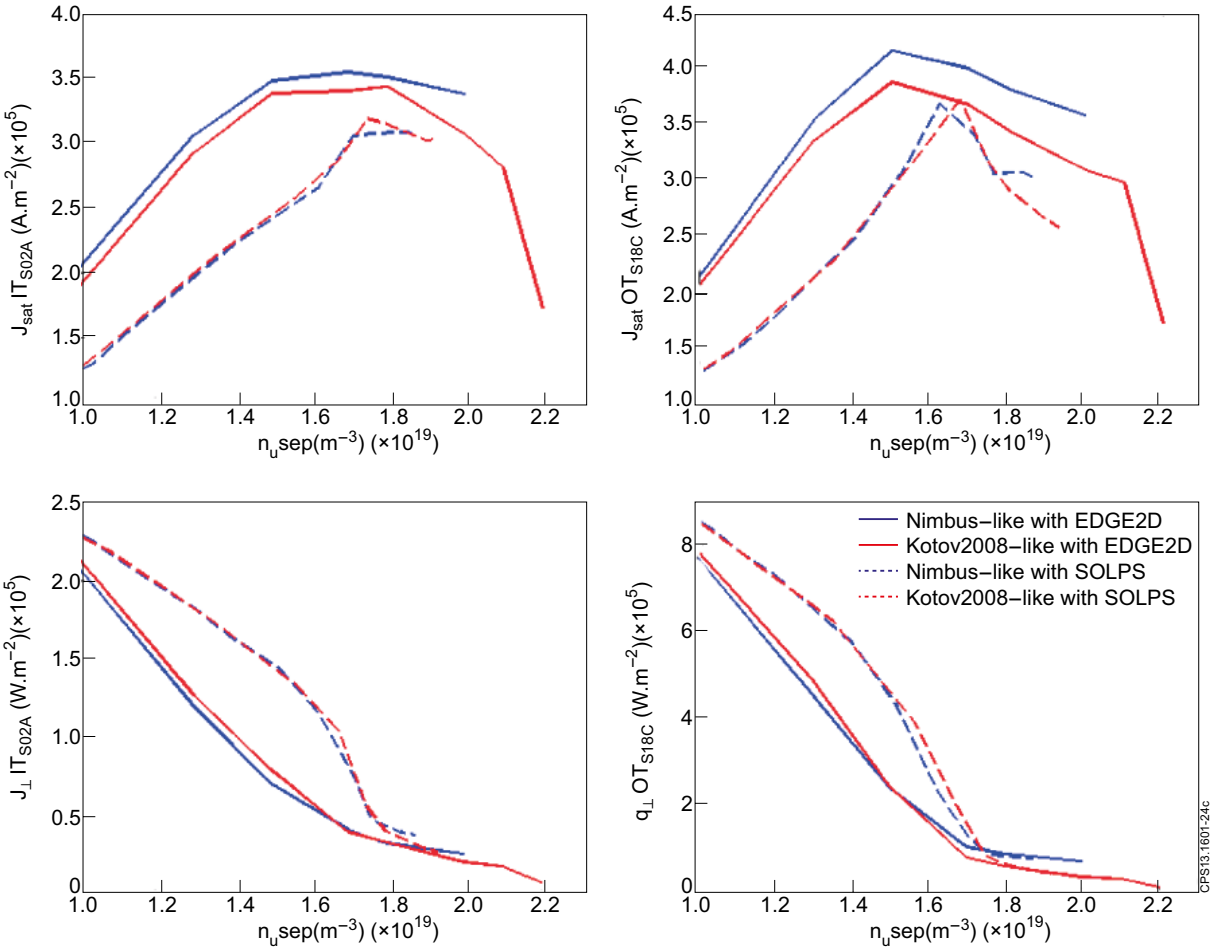

Figure 24: Comparison between EDGE2D-EIRENE and SOLPS4.3 simulations for a JET-C density ramp. Upper row from left to right: integral J_{sat} across the IT and OT. Lower from left to right: as above but for $q_\perp$.

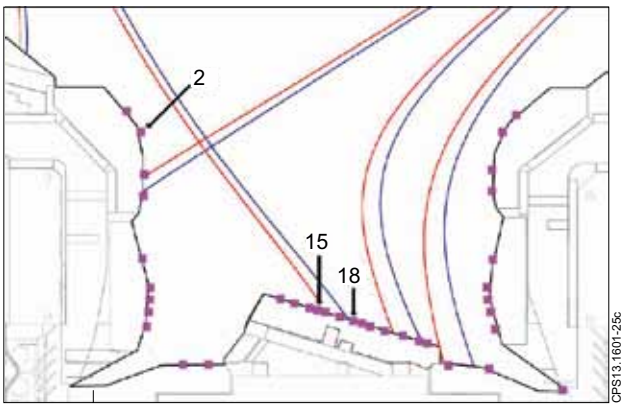

Figure 25: Probe numbers and positions used here (02 and 18) and in Section 8 (02, 15 and 18).

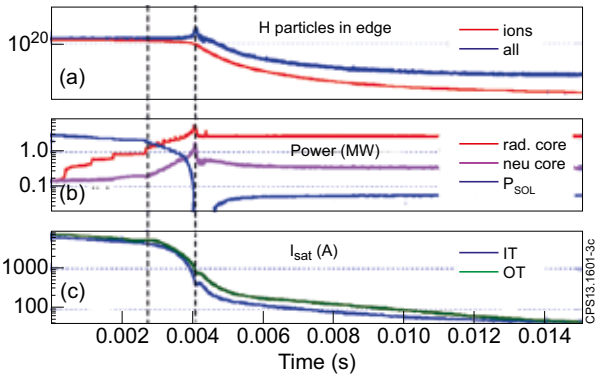

Figure 26: Evolution during the run "collapse" of the (a) H particle content (ions and ions+neutrals) outside the separatrix; (b) power balance in the core (total radiation, radiation from H neutrals, P_{SOL}; (c) Integral J_{sat} on the inner (IT) and outer (OT) targets.

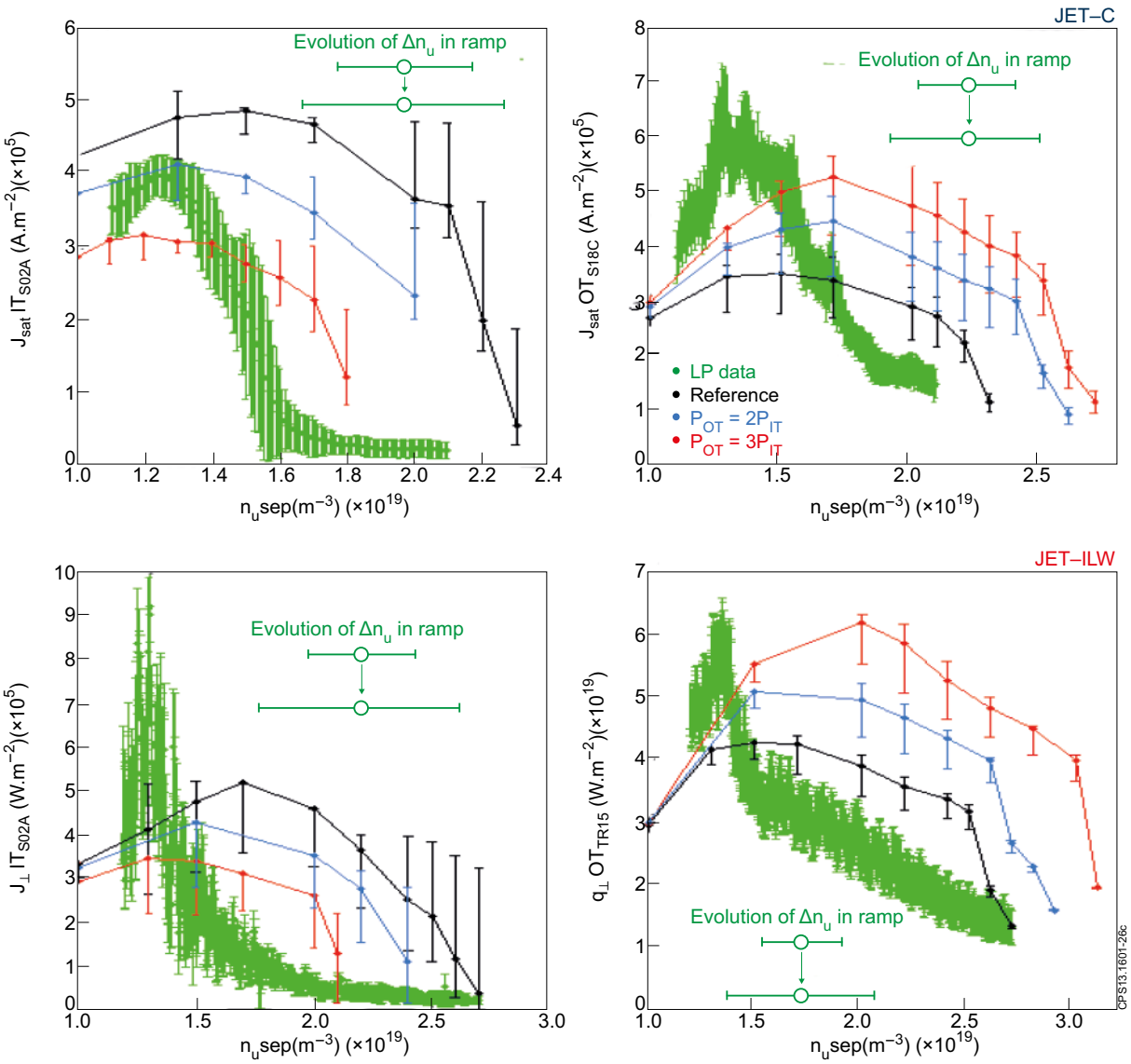

Figure 27: Comparison between EDGE2D-EIRENE simulations and experimental data for the J_{sat} at a given location in the SOL during the JET-C (upper) and JET-ILW (lower) density ramps. The reference model is the one presented in Section 3.

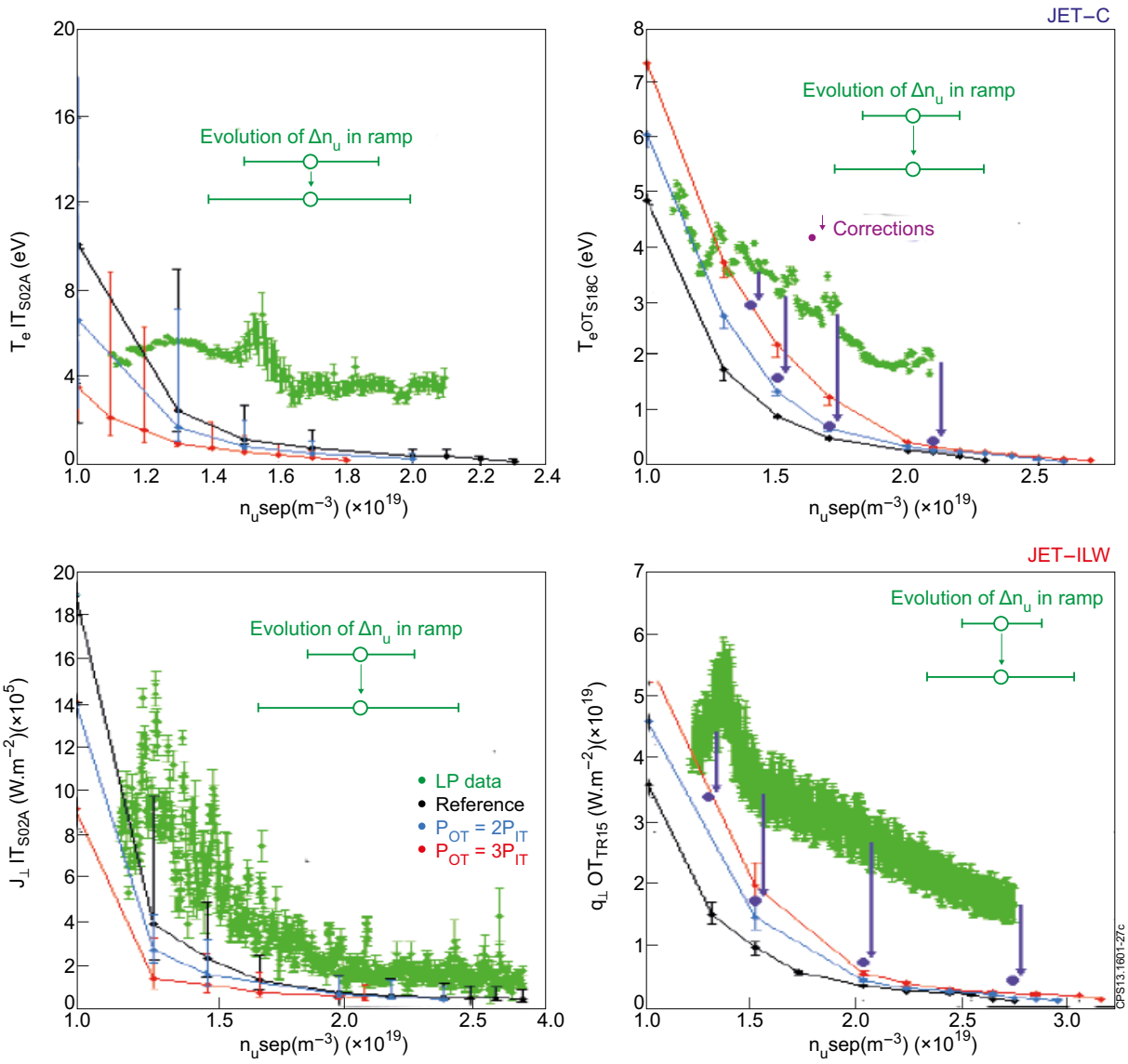

Figure 28: The same as Fig.27 but for target Te values on individual, magnetically connected probes.